

Pigment Organization and Transfer of Electronic Excitation in the Photosynthetic Unit of Purple Bacteria

Xiche Hu, Thorsten Ritz, Ana Damjanović, and Klaus Schulten*

Beckman Institute and Department of Physics, University of Illinois at Urbana-Champaign, Urbana, Illinois 61801

Received: November 13, 1996; In Final Form: February 24, 1997[®]

Absorption of light by light-harvesting complexes and transfer of electronic excitation to the photosynthetic reaction center (RC) constitute the primary light-harvesting process of photosynthesis. This process is investigated on the basis of an atomic level structure of the so-called photosynthetic unit of the photosynthetic bacterium *Rhodobacter sphaeroides*. The photosynthetic unit combines in the intracytoplasmic membrane a nanometric assembly of three pigment–protein complexes: (i) the photosynthetic reaction center, (ii) a ring-shaped light-harvesting complex LH-I, and (iii) multiple copies of a similar complex, LH-II. The unit has been modeled using the known structure of (i) and for (ii) a model structure complexed appropriately with (i); for (iii) the structure of LH-II of *Rhodospirillum molischianum* is substituted. The model describes in detail the organization of chromophores involved in primary light absorption and excitation transfer: a hierarchy of ring-shaped bacteriochlorophyll aggregates that surround four centrally located bacteriochlorophylls of the photosynthetic reaction center. The bacteriochlorophylls involved in the overall transfer are found in a coplanar arrangement. On the basis of the modeled structure a quantum-mechanical description of the entire light-harvesting process is developed. For this purpose an effective Hamiltonian is established *a priori* and then employed to describe the LH-II → LH-II → LH-I → RC cascade of excitation transfer. The transfer times calculated are in agreement with measured transfer times. The results suggest that excitons are the key carriers of the excitation transferred; i.e., electronic excitations are coherently delocalized in the photosynthetic unit. This suggestion is corroborated by an investigation of the effect of inhomogeneous broadening on the predicted excitons in LH-II and LH-I, an effect that is found to be significant but small. A particularly important role is played by the lowest energy excitons to which the circular arrangement of bacteriochlorophylls imparts vanishing oscillator strength. Despite the lack of oscillator strength, the low-energy excitons are well suited for exciton transfer on a subpicosecond and picosecond time scale. The accessory bacteriochlorophylls of the photosynthetic reaction center are found to be critical for the LH-I → RC transfer, which would take several hundred picoseconds without these bacteriochlorophylls.

1. Introduction

Absorption of photons by light-harvesting complexes (LHs) and transfer of excitation energy from LHs to the photosynthetic reaction center (RC) constitute the primary process of photosynthesis in bacteria and plants.^{1–4} In the early 1930s, Emerson and Arnold⁵ demonstrated that it took on average 2480 chlorophylls to fix one molecule of CO₂ under saturating flash intensity, indicating that only very few chlorophylls (RCs) take directly part in photochemical reactions. Most chlorophylls serve as light-harvesting antennae capturing the sunlight and funneling the electronic excitation toward the RC.^{6–9} The latter process is organized in so-called photosynthetic units (PSUs), which each consist of a RC and associated pigments, the light-harvesting complexes, that contain chlorophylls and, as accessory chromophores, carotenoids.^{9–12}

The RC possesses light-absorbing chlorophylls itself; however, photons absorbed by the RC chlorophylls are not sufficient to saturate its maximum turnover rate. When exposed to direct sunlight, chlorophylls absorb at a rate of at most 10 Hz and, in dim light, at a rate of 0.1 Hz. However, the RC can “turn over” at 1000 Hz.^{10,13} Light-harvesting complexes fuel excitation energy to the RC, which keeps the RC running at an optimal rate. In fact, excitation transfer from the light-harvesting complexes to the RC can increase the efficiency of energy utilization in photosynthesis by 2 orders of magnitude and,

through the accessory chromophores, also broadens the spectral range of light used.

A wealth of evidence has accumulated that proves that the organization of PSUs, to surround a RC by aggregates of chlorophylls and carotenoids, is universal in both purple bacteria and higher plants.^{11,14–16} The main principles governing the primary processes of photosynthesis most likely are similar for purple bacteria and photosystems of higher plants.^{16,17} The present article focuses on the PSU of purple bacteria that is located in intracytoplasmic membranes.¹⁸

The function of the bacterial RC is well understood, in no small measure due to the solution of its three-dimensional structure.^{19,20} The associated light-harvesting process, which funnels light energy within about 100 ps and near 95% efficiency to the RC, is much less understood due to a lack of structural information about the light-harvesting complexes in the bacterial PSU. This situation changed recently with the discovery of high-resolution crystal structures of two light-harvesting complexes in purple bacteria.^{21,22} These structures allow one to discern the pathways of excitation transfer and the underlying transfer mechanisms.

In most purple bacteria, the photosynthetic membranes contain two types of light-harvesting complexes, light-harvesting complex I (LH-I) and light-harvesting complex II (LH-II). Both complexes are trans-membrane proteins. LH-I is found surrounding directly the RCs, while LH-II is not directly associated with the reaction centers but transfers energy to the reaction

[®] Abstract published in *Advance ACS Abstracts*, April 15, 1997.

centers via LH-I.^{14,23} For some bacteria, such as *Rhodopseudomonas acidophila* and *Rhodospirillum molischianum* strain DSM 120,²⁴ there exists a third type of light-harvesting complex, LH-III. A fixed stoichiometry exists between RC and LH-I.¹⁴ However, the number of LH-IIs and LH-IIIs varies according to growth conditions such as light intensity and temperature.^{14,23}

All light-harvesting complexes are constructed in a remarkably similar fashion.^{14,25} The basic structural unit is a heterodimer of two short peptides (trans-membrane helices), commonly referred to as α -apoprotein and β -apoprotein; the two helices, in aggregating into the heterodimer, bind noncovalently bacteriochlorophylls (BChls) and carotenoids. Several heterodimers form larger circular aggregates that constitute the light-harvesting complexes. The size of the complexes differs for LH-I and LH-II and is species dependent. LH-IIIs from *Rps. acidophila* and *Rhodovulum sulfidophilum* were determined by X-ray crystallography²¹ and electron microscopy²⁶ to be nanomers of the $\alpha\beta$ -heterodimers. The crystal structure of LH-II from *Rs. molischianum* displayed an octamer.²² An 8.5 Å resolution electron microscopy projection map showed LH-I of *Rhodospirillum rubrum* to be a hexadecamer of the $\alpha\beta$ -heterodimers.²⁷

Purple bacteria contain bacteriochlorophyll a (BChl-a) or bacteriochlorophyll b (BChl-b) as the dominant chromophore, in addition to carotenoids. The majority of the widely studied purple bacteria are BChl-a containing species, such as *Rhodobacter sphaeroides*, *Rps. acidophila*, *Rs. rubrum*, and *Rs. molischianum*; an exception is *Rhodopseudomonas viridis*, which contains BChl-b.

Carotenoids exercise two functions in the PSU: (i) to protect chlorophylls from photooxidation by quenching the chlorophyll triplet state into their own triplet state, which lies low enough to prevent further transfer to oxygen; (ii) to absorb sunlight in a spectral region complementary to that of chlorophylls²⁸ and to funnel this energy into the PSU's light-harvesting system. Interestingly, the carotenoids seem to engage for the latter purpose also their low-lying triplet state in that they convert an optically allowed state at 500 nm into an optically forbidden singlet state near 800 nm, which is typical for polyenes and composed of two triplet excitations.^{29,30}

In case of LH-II, the $\alpha\beta$ -heterodimer binds three BChls and one to two carotenoids noncovalently. Two of the three BChls absorb at a wavelength of 850 nm, and the other absorbs at 800 nm. The $\alpha\beta$ -heterodimer of LH-I contains solely one pair of BChls absorbing at 875 nm and one carotenoid. There exists a pronounced energetic hierarchy in the light-harvesting system: LH-III absorbs light at the highest energy (800 and 820 nm);^{31,32} the LH-II complex, which surrounds LH-I, absorbs maximally at 800 and 850 nm; LH-I, which in turn surrounds the RC, absorbs at a lower energy (875 nm).¹⁴ The energy cascade serves to funnel electronic excitations from the LH-IIIs and LH-IIs through LH-I to the RC.

To understand the mechanism for excitation transfer within the PSU, structural information of each component as well as information on the overall assembly of light-harvesting complexes is required. In this paper we investigate the PSU of *Rb. sphaeroides*, which does not contain LH-III. Structures of the RC are known for *Rp. viridis*¹⁹ as well as for *Rb. sphaeroides*.^{20,33} As mentioned above, structures of LH-II are available for *Rps. acidophila*²¹ and for *Rs. molischianum*.²² Structures of LH-I of any species had been lacking, although an 8.5 Å resolution projection map observed by electron microscopy was reported for LH-I of *Rs. rubrum*.²⁷ On the basis of a high degree of homology of the $\alpha\beta$ -heterodimer of LH-I from *Rb. sphaeroides* to that of LH-II of *Rs. molischianum*,^{24,34} an atomic

structure for the respective LH-I has been modeled³⁵ in agreement with the observed projection map for LH-I of *Rs. rubrum*.²⁷ Thus, a structural model for the bacterial PSU consisting of LH-IIIs, LH-I, and the RC is established at atomic resolution.

The structures mentioned provide detailed knowledge of the organization of chromophores in the photosynthetic membrane and open an avenue for a study of excitation transfer in the PSU based on *a priori* principles. This article describes such study investigating the mechanisms of excitation transfer in the PSU at two levels: excitation transfer within each individual pigment–protein complex and excitation transfer among pigment–protein complexes. The investigation is based on quantum-mechanical calculations.

The remainder of this article is organized as follows. Section II describes the molecular model of the bacterial PSU, with particular emphasis on the pigment organization. The crystal structure of LH-II from *Rs. molischianum* is reviewed in light of newly reported resonance Raman spectra on site-mutated LH-I of *Rb. sphaeroides* and the structure of LH-I surrounding the RC is described. Sections III and IV discuss intracomplex and intercomplex excitation transfer. A conclusion is given in section V.

2. Structures of Light-Harvesting Complexes and of the Photosynthetic Unit

The PSU combines in the intracytoplasmic membrane of purple bacteria a nanometric assembly of the photosynthetic reaction center and ring-shaped light-harvesting complexes. In this section we describe a model of the PSU of *Rb. sphaeroides* that is based on the known structure of the RC of that species, substitutes for the species' LH-II an LH-II of *Rs. molischianum*, and employs a computationally modeled structure of LH-I based on its high-sequence homology to LH-II of *Rs. molischianum*. The LH-I is known to form a ring around the RC, and a corresponding complex is assumed here. The LH-I complex with the RC is then combined with several LH-IIIs. The final arrangement of the light-harvesting complexes yields the detailed organization of chromophores involved in primary light absorption and excitation transfer in the PSU: a hierarchy of ring-shaped BChl aggregates surround four centrally located BChls of the photosynthetic reaction center. The BChls involved in the overall transfer are found in a coplanar arrangement that is optimal for the unidirectional flow of excitation energy toward the reaction center. The modeled structure will be used further below to develop a quantum-mechanical description of the entire light-harvesting process in the PSU. We will first discuss the structure of LH-II, commenting in particular on a network of hydrogen bonds that fixes the geometry of the B850 BChls aggregate. We discuss then the structure of the complex of LH-I and the RC that has been derived in ref 35. We describe briefly how LH-I and LH-II have been aggregated and comment then on the overall organization of BChls in the PSU.

Structure of LH-II. A 2.4 Å resolution structure of the light-harvesting complex II (LH-II) of *Rs. molischianum* had been reported in ref 22. As shown in Figure 1a, the complex is an octameric aggregate of $\alpha\beta$ -heterodimers, the latter noncovalently binding three BChl-a molecules and one lycopene. Two concentric cylinders of helical protein subunits, with the α -apoproteins inside and the β -apoproteins outside, form a scaffold for the BChls. Sixteen B850 BChl molecules form a continuous overlapping ring of 23 Å (radius) with each BChl oriented perpendicular to the membrane plane and sandwiched between the helical apoproteins. The Mg–Mg distance between neighboring B850 BChls is 9.2 Å within the $\alpha\beta$ -heterodimer and 8.9 Å between the heterodimers. Eight B800 BChls,

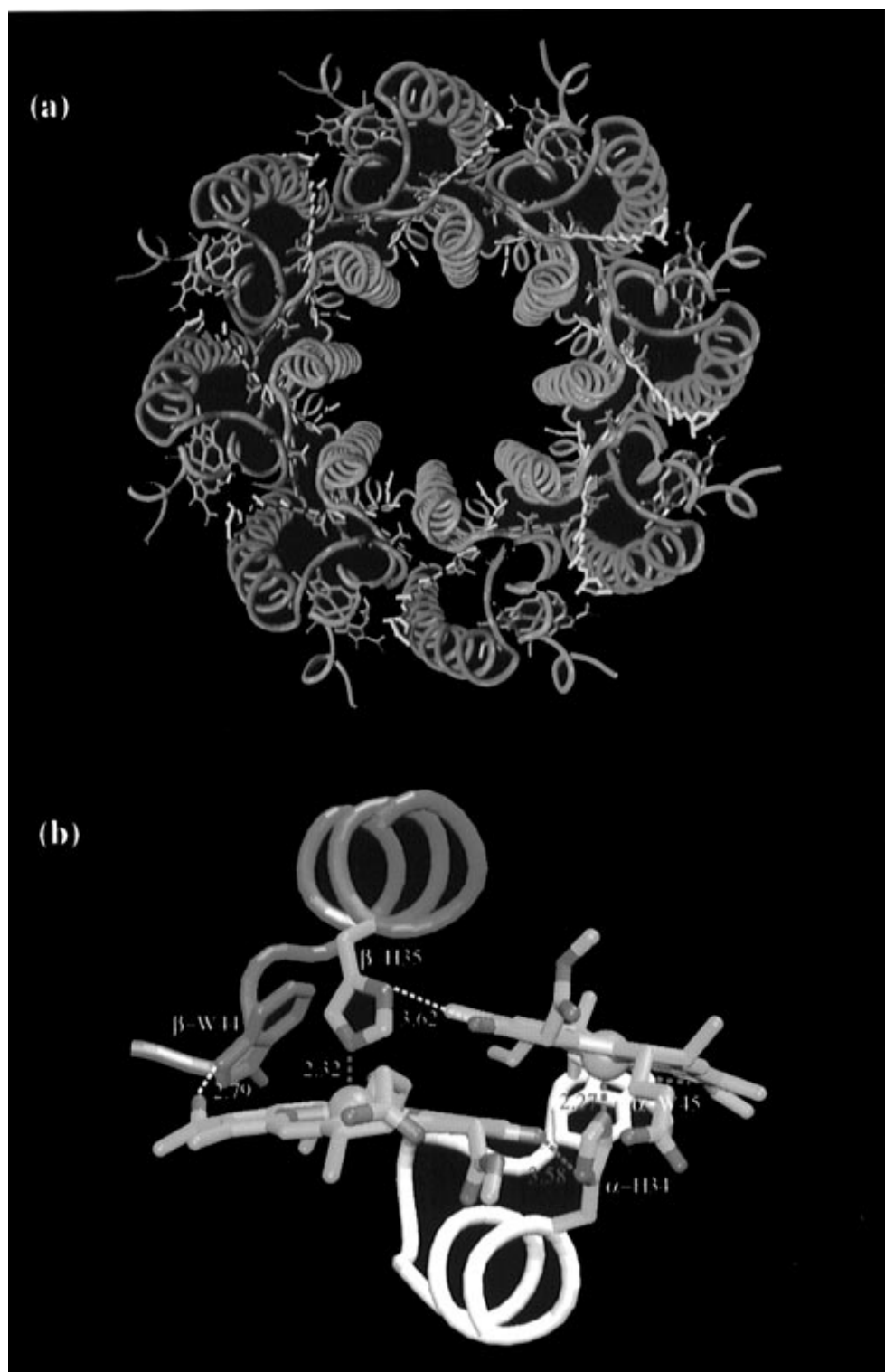


Figure 1. (a) LH-II octameric complex of *Rs. molischianum*.²² This image displays a top view with N-terminal pointing upward, the apoproteins are represented as C_α -tracing tubes with the α -apoproteins (inside) in cyan and the β -apoprotein (outside) in magenta. The BChl-a molecules are in green with phytol tails truncated for clarity. The lycopenes are in yellow. (b) B850 BChls in the $\alpha\beta$ -heterodimer of LH-II of *Rs. molischianum*.²² The α -apoprotein (white) and the β -apoprotein (magenta) are represented as C_α -tracing tubes. Dashed lines indicate metal–ligand or hydrogen bonds between BChl and protein side chain atoms with numbers labeling distances in Å. Central Mg atoms are represented as van der Waals spheres. (Produced with the program VMD.⁷²)

forming another ring of 28 Å, are arranged nearly parallel to the membrane plane with the tetrapyrrole rings and exhibit a Mg–Mg separation of 22 Å between neighboring BChls. The ligation sites for the B850 BChl are α -His-34 and β -His-35, while the B800 BChls ligate to α -Asp-6. Eight lycopene molecules span the transmembrane region, making contact with B800 BChl and one of the two B850 BChls.

Resonance Raman spectra on LH-II of *Rs. molischianum* suggested that the 9-keto group may be hydrogen bonded.²⁴ As reported previously,²² the electron density map shows no potential hydrogen bond donor within hydrogen bond distance to the O₁ atom of the 9-keto groups of B850 BChls. However, an examination of the crystal structure shows that the two histidine residues α -His-34 and β -His-35, which bind the central

Mg atoms of the B850 BChls, can actually be involved in hydrogen bonding of the 9-keto group of the B850 BChls. In fact, the distance between the $N_{\delta 1}$ atom of β -His-35 and the 9-keto oxygen of B850a BChl is 3.62 Å, and the distance between the $N_{\delta 1}$ atom of α -His-34 and the 9-keto oxygen of B850b BChl is 3.58 Å. (We adopt here the notation of B850a and B850b introduced in ref 22, for labeling the B850 BChls that bind to the α -apoprotein and the β -apoprotein, respectively.) These distances are depicted in Figure 1b. The suggested hydrogen bonds are consistent with recent results of resonance Raman spectra of different mutants of LH-I of *Rb. sphaeroides*.³⁶ Vibrations in the 1600–1700 cm^{−1} region are known to be associated with the stretching modes of the conjugated carbonyl group, i.e., the 2-acetyl and the 9-keto groups of BChl-a.³⁷ The peak frequency for the unbounded 9-keto group is around 1700 cm^{−1}. The peak shifts by −40 cm^{−1} upon hydrogen bonding. This characteristic peak for the hydrogen-bonded 9-keto group has been observed in the resonance Raman spectra of LH-I from *Rb. sphaeroides*.³⁶ Since LH-I of *Rb. sphaeroides* is highly homologous to LH-II of *Rs. molischianum* and the resonance Raman spectra of the two complexes are strikingly similar,²⁴ the crystal structure of LH-II from *Rs. molischianum* was used to guide the site-directed mutation experiment. When all the potential hydrogen bonding side chains, except the Mg-binding histidines, in the immediate surroundings of the 9-keto group were mutated, the characteristic hydrogen-bonded 9-keto Raman peak was not affected. However, when the histidine residues were mutated the characteristic Raman peak disappeared.³⁶ We suggest, therefore, that the central Mg-binding histidine residues also formed hydrogen bonds with the 9-keto groups of the B850 BChls in LH-II of *Rs. molischianum*.

According to the suggestion made, each B850 BChl is noncovalently bound to three side chain atoms of the α - or the β -apoprotein. Figure 1b shows all the bonding partners of the two B850 BChls in the $\alpha\beta$ -heterodimer. In the case of B850a BChl, the central Mg atom is bonded to the $N_{\epsilon 2}$ atom of α -His34, the 2-carboxyl group is hydrogen bonded to the $N_{\epsilon 1}$ atom of α -Trp45, and the 9-keto group is hydrogen bonded to the $N_{\delta 1}$ atom of β -His-35. In the case of B850b BChl the central Mg atom is bonded to the $N_{\epsilon 2}$ atom of β -His35, and the 2-carboxyl and the 9-keto groups are hydrogen bonded to the $N_{\epsilon 1}$ atom of β -Trp44 and the $N_{\delta 1}$ atom of α -His-34, respectively. One may notice in this respect that it takes three bonds to prevent any rotation of the BChl moieties; i.e., apparently, the orientation of the B850 BChl is spatially well defined in LH-II. The resulting geometrical stability of BChl may contribute to a geometrical rigidity of the BChl aggregate, which has implications for the mechanism of light energy transfer and possibly also for the aggregation and size of light-harvesting complexes.

Structure of the LH-I Complex with the Photosynthetic Reaction Center. A structure of LH-I of *Rb. sphaeroides* has been modeled in ref 35 and yielded an electron density projection map in agreement with the 8.5 Å resolution electron microscopy projection map for LH-I of *Rs. rubrum*.²⁷ The overall diameter of the LH-I complex is 118 Å. The complex contains a ring of 32 BChls referred to as B875 BChls according to their main absorption band. The Mg–Mg distance between neighboring B875 BChls is 9.2 Å within the $\alpha\beta$ -heterodimer and 9.25 Å between neighboring heterodimers.

A model for the LH-I–RC complex was subsequently built. Coordinates of RC were taken from the 2.65 Å resolution structure of the photosynthetic reaction center of *Rb. sphaeroides* (PDB accession number:1PCR) as published in ref 33. To search for the minimum energy conformation, the RC structure was placed inside the LH-I ring and was allowed to rotate and

translate as a rigid body. A unique minimum was reached for the LH-I–RC complex,³⁵ which corresponds to a coplanar arrangement of lipid-exposed tryptophane side groups of LH-I and of RC.

Relative Arrangement of LH-I and LH-II. In order to obtain a complete atomic resolution structure of a PSU consisting of LH-IIs, LH-I, and the RC, we aligned the two complexes through a common plane defined by the planes of lipid-exposed tryptophans in both the LH-I–RC complex and the LH-II complex.³⁵ The complexes were then arranged as shown in Figure 2a, choosing the β -apoproteins to interdigitate partially. The final arrangement was obtained through minimization of the van der Waals interaction between the complexes, keeping the complexes fixed in the common plane. The resulting shortest Mg–Mg distance measures about 24 Å between neighboring LH-IIs and 22 Å between LH-I and LH-II.

Pigment Organization. Figure 2b presents the positions and orientations of all the bacteriochlorophylls for an assembly of an LH-II in contact with an LH-I that surrounds a RC. The closest distance between the central Mg atom of the RC special pair (chlorophylls P_A, P_B) and the Mg atom of the LH-I BChls is 42 Å. The distance between the Mg atom of the accessory BChl (chlorophylls B_A, B_B) and the LH-I BChls is shorter, the nearest distance measuring 35 Å. Both LH-I and LH-II feature rings of BChls that are positioned near the periplasmic side of the membrane. Most importantly, the B850 BChls of LH-II and the B875 BChls of LH-I are all exactly coplanar. Interestingly, the plane of the BChls encompasses the reaction center special pair (P_A and P_B) and the so-called accessory BChls (B_A, B_B). Such planar pigment organization appears to be optimal for energy transfer from the outer light-harvesting complexes to the RC.

The PSU of purple bacteria combines a RC with multiple light-harvesting complexes. The latter contain one or two rings of BChls absorbing in the range 800–900 nm and carotenoids absorbing around 500 nm. Figure 3 depicts the energy levels for the key electronic excitations of the chromophores in the PSU. The energy levels form a funnel that channels electronic excitation toward the RC, the sink of the energy. The excitation transfer processes cascading into the RC can be classified into intracomplex and intercomplex excitation transfer, defined as excitation transfer within each pigment protein complex (LH-II, LH-I, RC) and between pigment protein complexes (LH-II → LH-II, LH-II → LH-I, LH-I → RC), respectively. Due to the closer proximity of chromophores within each pigment protein complex, intracomplex excitation transfer usually occurs faster than intercomplex excitation transfer. As a result, the electronic excitation of the lowest energy within each pigment protein complex becomes populated before a complex transfers the excitation further.

3. Primary Processes in LH-II

LH-II contains two types of BChls, B800 and B850, as well as lycopenes, a particular carotenoid. Figure 4 shows the arrangement of these chromophores in LH-II of *Rs. molischianum*. The chromophores form a tight circular aggregate of 16 B850 BChls and 2 loose aggregates of 8 B800 BChls and 8, possibly more, lycopenes. Excited B800 BChl transfers its electronic excitation to the ring of B850 BChls. Time-resolved spectroscopy has shown that this excitation transfer process occurs on a subpicosecond scale.^{1,38–42} The excitation transfer, in principle, can arise from two mechanisms, one involving induced dipole–induced dipole coupling and referred to as the Förster mechanism⁴³ and the other involving electron exchange and referred to as the Dexter mechanism.⁴⁴

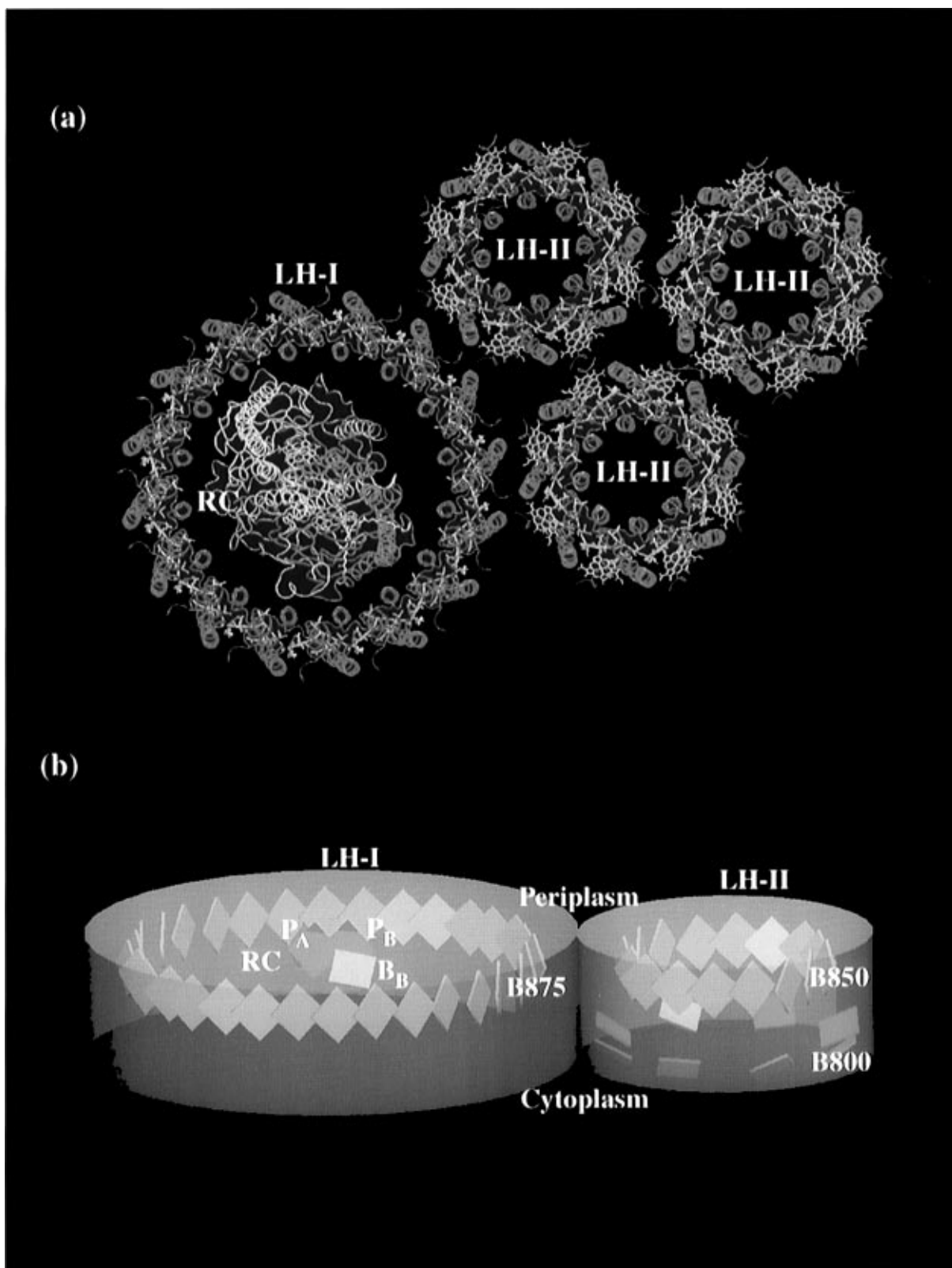


Figure 2. (a) Arrangement of pigment protein complexes in the modeled bacterial photosynthetic unit (PSU) of *Rb. sphaeroides*. The α -helices are represented as α -tracing tubes with α -apoproteins of both LH-I and LH-II in blue and β -apoproteins in magenta, and the L, M, H subunits of RC in yellow, red, gray respectively. All the BChls are in green, and carotenoids are in yellow. (b) Pigment organization in a minimum photosynthetic unit consisting of RC, LH-I, and LH-II. Bacteriochlorophylls are represented as squares. LH-II contains two types of BChls commonly referred to as B800 (dark blue) and B850 (green) which absorb at 800 and 850 nm, respectively. BChls in LH-I absorb at 875 nm and are labeled as B875 (green). P_A and P_B refer to the reaction center special pair, and B_A , B_B to the accessory BChls. The figure exhibits clearly the coplanar arrangement of the B850 BChl ring in LH-II, the B875 BChl ring of LH-I, and the reaction center BChls P_A , P_B , B_A , B_B . (Produced with the program VMD.⁷²)

The Förster mechanism is operative over long distances (≤ 40 Å), requires that the excitations involved be optically allowed, and is most efficient when the transition dipole moments of

the BChl Q_y excitations involved are collinear or at least parallel.¹ The Dexter mechanism⁴⁴ requires, to be effective, significant overlap of donor and acceptor wave functions, i.e.,

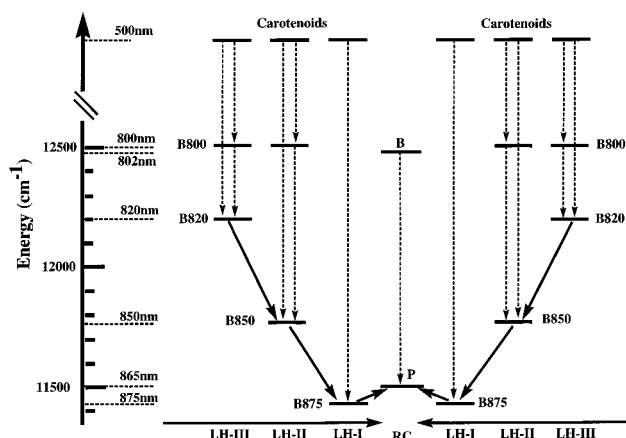


Figure 3. Energy levels of the electronic excitations in the PSU of purple bacteria with BChl-a. The diagram illustrates a funneling of excitation energy toward the photosynthetic reaction center (RC). The dashed lines indicate (vertical) intracomplex exciton transfer, the solid lines (diagonal) intercomplex energy transfer. LH-I exists in all purple bacteria; LH-II exists in most species; LH-III arises in certain species only.

requires a close contact between donor and acceptor. Although there is no direct contact between B800 BChls and B850 BChls, the Dexter mechanism may be realized through exchange mediated by a lycopene: the $2A_g$ state in lycopene discussed below, which is in energetic proximity to the Q_y state of the B800 system, may serve as a carrier. Figure 5 shows that the lycopene runs parallel (within 5 Å) to the porphyrin plane of a B850a BChl and makes van der Waals contact with a B800 BChl.

The Role of the B800 System in LH-II. The B800 system in LH-II absorbs mainly red light into its Q_y state and funnels its excitation to the B850 system. One can discern in Figure 4 that the transition dipole moments of the Q_y states of a particular B800 BChl and that of its most proximate B850b and B850a' (cf., Figure 4) chlorophylls form angles of 13.1° and 151.5°, respectively; i.e., they are nearly parallel. The Q_y transition dipole in BChl is collinear with the axis connecting the molecule's N atom of pyrrole I to the N atom of pyrrole III.^{45,46} The Mg–Mg distances between B800 BChl and B850b and B850a' are 20.2 and 19.1 Å, respectively; i.e., they are well within the operative range of the Förster mechanism.¹

It has been suggested, however, that subpicosecond excitation transfer involving BChls cannot solely rely on the Förster mechanism.¹ Single mutation (α -Tyr44 → Phe) and double mutation (α -Tyr44, Tyr-45 → Phe, Leu) in LH-II of *Rb. sphaeroides* resulted in a progressive blue shift of the B850 band to 838 and 826 nm.⁴⁷ The observed excitation transfer rate correlates with this spectral blue shift in qualitative accordance with the Förster spectral overlap formula, but the variation of the rate is wider than predicted by the Förster mechanism.⁴⁸ The discrepancy may be indicative of a contribution to the B800 → B850 excitation transfer beyond the Förster mechanism.

The Role of Lycopene. The antenna function of carotenoids has been reviewed in refs 49 and 50. In LH-II, lycopene absorbs light near 500 nm into a strongly allowed excited state. This state, however, is completely out of resonance with the BChl Q_y excitations that are thought to be the accepting states of excitations from LH-II carotenoids. The fundamental issue arises as to how the 500 nm excitation can be channeled to Q_y excitations of BChls. Figure 5 compares the excitation energies of lycopene and the BChls in LH-II of *Rs. molischianum*. The figure indicates that in lycopene exist two low-lying singlet

excited states S_1 and S_2 . Due to an approximate C_{2h} symmetry these states may be labeled $2A_g$ and B_u in analogy to these states in polyenes^{30,51} where the symmetry applies. Similarly, an A_g symmetry label can be associated with the ground state. Due to these approximate symmetries, the state S_2 (B_u) of lycopene is optically allowed and absorbs the light energy; the state S_1 ($2A_g$) is optically forbidden, strongly so despite a breaking of the C_{2h} symmetry in lycopene. The $2A_g$ appears to be crucial for the photodynamics of polyenes. In fact, in β -carotene with the same number of conjugated double bonds as lycopene, the B_u state is extremely short lived after optical excitation with a lifetime of (195 ± 10) fs,⁵² the $2A_g$ becoming populated instead. Thus, the $2A_g$ state is actually excited through 500 nm photons, albeit indirectly. The $2A_g$ itself exhibits, however, a relatively short lifetime of (10 ± 2) ps.⁵³

The $2A_g$ states in polyenes are well characterized,^{30,51} e.g., through fluorescence from this state after initial absorption to S_2 . However, fluorescence from $2A_g$ becomes undetectable for long chains (number of conjugated double bonds exceeding 10) due to the widening of the $2A_g$ to B_u energy gap with increasing chain length, which slows down the internal conversion $B_u \rightarrow 2A_g$, and due to a decrease of the gap to the ground state, which increases the rate of internal conversion; as a result, no direct measurement of the $2A_g$ energy level is available for carotenoids. For a long time, the energy level for the $2A_g$ state was estimated to be at $17\ 230\ \text{cm}^{-1}$.⁴⁹ Recently, however, the $2A_g \rightarrow 1A_g$ fluorescence has been measured for polyenes with 11 conjugated double bonds, placing the 0–0 origin of the $2A_g \rightarrow 1A_g$ transition at $13\ 100\ \text{cm}^{-1}$ in *n*-hexane and at $12\ 800\ \text{cm}^{-1}$ in CS_2 .⁴⁹ It is noteworthy that the latter energy is close to the excitation energy for the Q_y transitions of B800 BChl ($12\ 500\ \text{cm}^{-1}$) and B850 BChl ($11\ 764\ \text{cm}^{-1}$) since lycopene itself has 11 conjugated double bonds. Low-lying singlet states of polyenes have been calculated by the PPP-MRD-CI (Pariser–Parr–Pople multireference double excitation configuration interaction) method for up to $n = 8$.³⁰ It has been found that the excitation energy of the $2A_g^-$ state of conjugated polyenes exhibits a linear dependence on $1/(2n + 1)$. Extrapolation of the linear relation to $n = 11$ leads to an estimate of the $2A_g$ excitation energy of $15\ 000\ \text{cm}^{-1}$ in *vacuo*. A solvent would reduce this value such that an excitation energy near $13\ 000\ \text{cm}^{-1}$ of lycopene in LH-II is also expected on theoretical grounds.

It thus appears that energy transfer from lycopene to the B800 and B850 BChl systems is feasible. The question arises if such transfer could proceed within a few hundred femtoseconds. Since the gateway for this transfer is the optically forbidden $2A_g$ state, the underlying transfer mechanism must be electron exchange. Evaluation of the strength of the respective coupling through configuration interaction expansions accounting for the doubly excited character of the $2A_g$ state revealed that the electron exchange (Dexter) mechanism, indeed, can be effective.⁵⁴ Further below we will demonstrate that the electronic excitations of the B850 system can readily accept energy from lycopene through local electron exchange. It is most remarkable that the scenario for lycopene → BChl excitation transfer and lycopene-mediated B800 → B850 excitation transfer invokes electron exchange, implying that electron transfer does not only play a fundamental role in the RC, but also in the light-harvesting complexes.

An alternative to lycopene → B850 (B800) energy transfer through a $2A_g$ gateway state is direct transfer from B_u to the Q_x state of BChl. The short lifetime (200 fs) of the B_u of carotenoids disfavors this route, but a relatively large transition dipole moment of lycopene may render the time scale of the

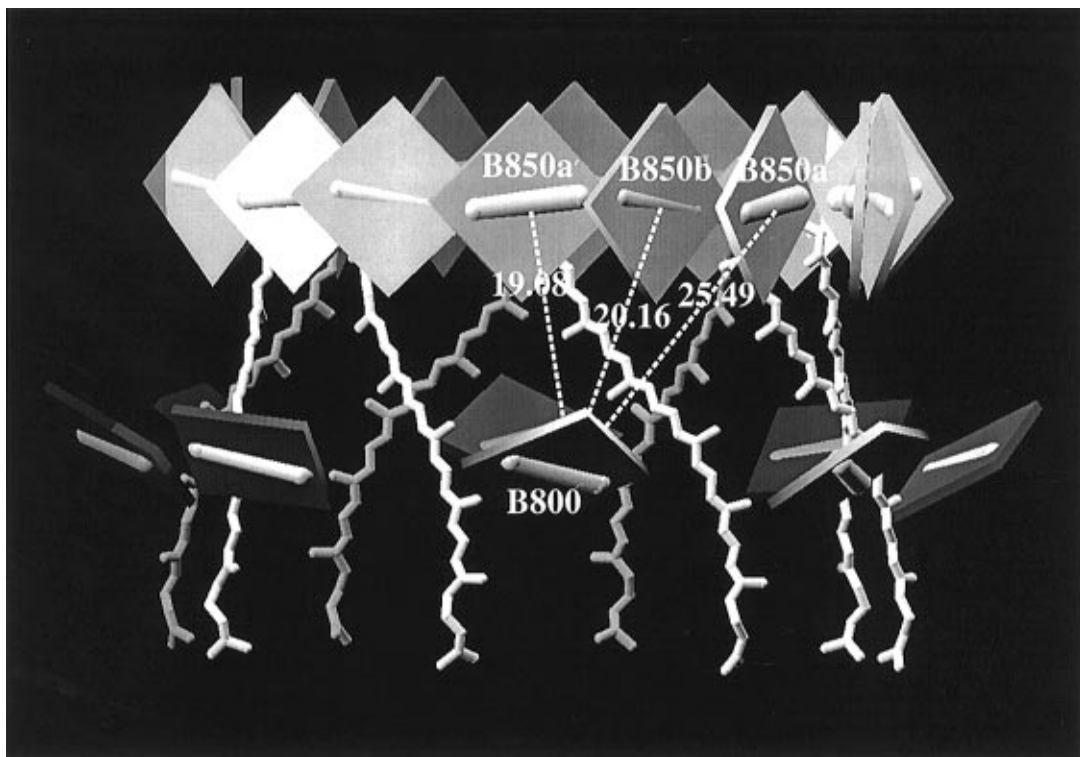


Figure 4. Arrangement of chromophores in LH-II of *Rs. molischianum*.²² Bacteriochlorophylls (BChls) are represented as squares; 16 B850 BChls are arranged in the top ring and 8 B800 BChls in the bottom ring. Carotenoids (lycenes) are shown in a licorice representation. Bars connected with the BChls represent the Q_y transition dipole moments. Representative distances between central Mg atoms of B800 BChl and B850 BChl are indicated (in Å). The B850 BChls bound to the α -apoprotein and the β -apoprotein are denoted as B850a and B850b, respectively; bacteriochlorophyll B850a' is bound to the (left) neighboring heterodimer. (Produced with the program VMD.⁷²)

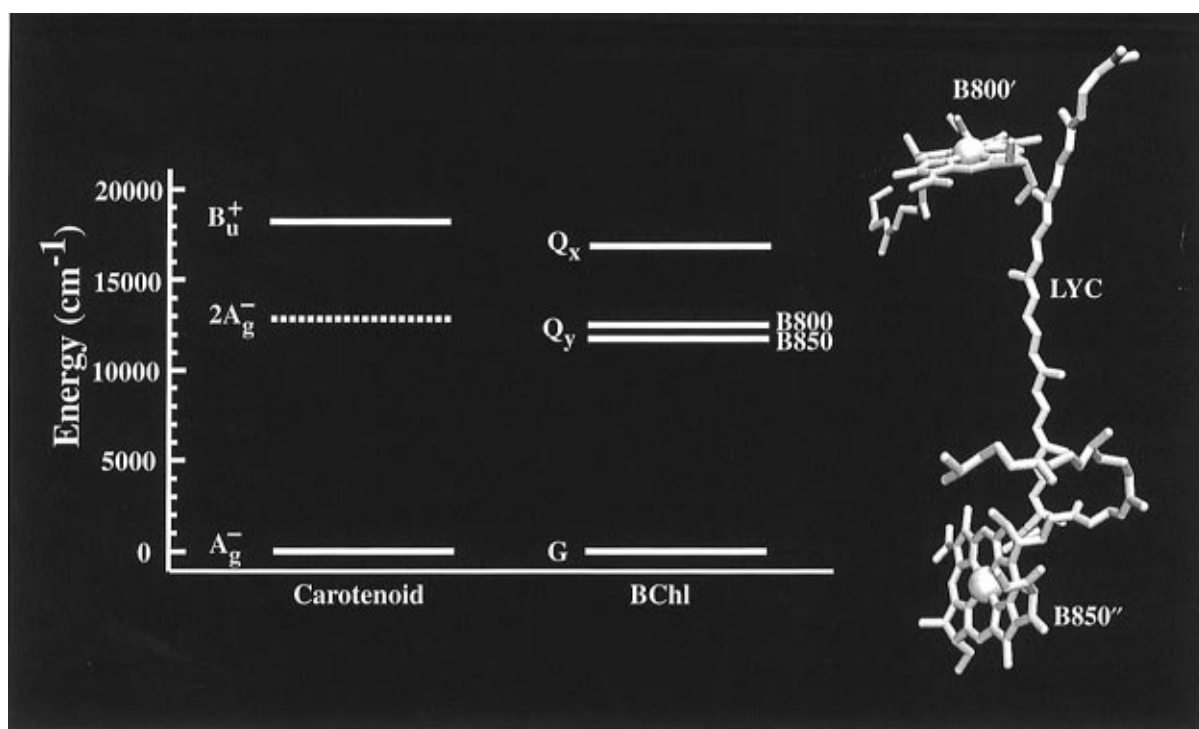


Figure 5. Contacts between B800, B850 BChls and lycopene (LYC) in LH-II as well as the energies of the electronic ground and excited states of the chromophores. Solid lines represent spectroscopically measured energy levels. The dashed line indicates the estimated energy of the $2A_g$ state of lycopene (carotenoid). B850a'' stands for the B850 BChl-a bound to the α -apoprotein of the right-hand side neighboring $\alpha\beta$ -heterodimer, and the B800' for the B800 BChl-a bound to the left-hand side neighboring $\alpha\beta$ -heterodimer.

excitation transfer B_u (lycopen) \rightarrow Q_x (BChl) as short as 200 fs, making this route at least partially efficient. In fact, recent work by Ricci et al. suggests that both internal conversion and direct transfer can occur on the same time scale.⁵⁵

4. Intercomplex Excitation Transfer

Having established the structure of the chromophore aggregates in LH-I and LH-II, one naturally seeks to investigate

how well this structure explains the observed excitation transfer characteristics in the PSU. We want to demonstrate in this section that an effective Hamiltonian can be provided that, albeit not exact, provides a satisfactory description of the excitation transfer involving the B850 and B875 BChls aggregates forming the PSU of *Rb. sphaeroides*.

We will proceed as follows. In a first step we will establish an effective Hamiltonian for the B850 ring system of LH-II. The Hamiltonian can be readily generalized to describe multiple LH-II rings as well as LH-I. In a second step we consider the effect of disorder which breaks the symmetry of the aggregates. Naturally, the mechanism of excitation transfer must be robust against naturally occurring structural and energetic fluctuations, and hence, the effect of such disorder must be investigated. In a third step, we investigate how energy is transferred between two LH-II rings and between an LH-II and an LH-I ring; i.e., we investigate the energy migration LH-II \rightarrow LH-II \rightarrow LH-I. In a fourth step, we describe the excitation transfer from the LH-I B875 system to the special pair of the RC. Finally, we return to the initial phase of the light-harvesting process involving lycopene \rightarrow B850 and B800 \rightarrow B850 transfers.

Definition of the Effective Hamiltonian. In order to establish an effective Hamiltonian for the circular BChl aggregate in LH-II, we assume that the relevant electronic excitations of the aggregate can be described in terms of single BChl Q_y excitations

$$|\alpha\rangle = \psi_1(g)\psi_2(g)\cdots\psi_{\alpha-1}(g)\psi_\alpha(Q_y)\psi_{\alpha+1}(g)\cdots\psi_{2N}(g) \quad (1)$$

Here, $\psi_j(g)$ describes the j th BChl in the electronic ground state and $\psi_\alpha(Q_y)$ describes the α th BChl in the Q_y excited state. $2N$ is the number of BChls in the aggregate, i.e., 16 in case of the B850 system of LH-II and 32 in case of the B875 system of LH-I. The states $|\alpha\rangle$ form an orthogonal basis such that

$$\langle\alpha|\alpha'\rangle = \delta_{\alpha\alpha'} \quad (2)$$

We need to account for interactions between the BChls that induce a migration of electronic excitation between the BChls. For chromophores j and k , not in close proximity, the leading term of the interaction is due to induced dipole-induced dipole coupling given by

$$W_{jk} = C \left(\frac{\vec{d}_j \cdot \vec{d}_k}{r_{jk}^3} - \frac{3(\vec{r}_{jk} \cdot \vec{d}_j)(\vec{r}_{jk} \cdot \vec{d}_k)}{r_{jk}^5} \right) \quad (3)$$

where \vec{d}_j are unit vectors describing the direction of the transition dipole moments of the ground state $\rightarrow Q_y$ state transition of the j th BChl and \vec{r}_{jk} is the vector connecting the centers of BChl j with BChl k . We consider \vec{d}_{jk} to be unit vectors since the magnitudes of the transition dipole moments of BChls are treated here as unknowns. The latter quantities would enter the expression for the matrix elements (3) together with a dielectric constant accounting for the optical density of the material; to account for the missing quantities we multiply the matrix element by an *a priori* unknown constant C to be determined through comparison with the detailed quantum-chemical calculations.⁵⁶ In case of proximate BChls, the coupling of local excitations cannot be captured by a simple formula like (3) that assumes in its derivation an abridged multipole expansion as well as the so-called zero-differential overlap approximation of atomic orbitals. Instead, we introduce the respective matrix elements as parameters to be determined below.

An evaluation of the dipolar coupling (3) requires knowledge of the positions of all BChls j , $j = 1, 2, \dots, 16$, as well as

knowledge of the unit vectors \vec{d}_j representing the orientation of transition dipole elements. These quantities are provided through the structure of LH-II as reported in ref 22. Table 2 presents the coordinates of the B850 BChls in LH-II of *Rs. molischianum* as well as the orientation of \vec{d}_j through an angle ϕ_j .

The Hamiltonian in the basis (1) for $k = 1, 2, \dots, 16$ can be written

$$\hat{H} = \begin{pmatrix} \epsilon & v_1 & W_{1,3} & W_{1,4} & \dots & . & W_{1,2N-1} & v_2 \\ v_1 & \epsilon & v_2 & W_{2,4} & \dots & . & W_{2,2N-1} & W_{2,2N} \\ W_{3,1} & v_2 & \epsilon & v_1 & \dots & . & W_{3,2N-1} & W_{3,2N} \\ W_{4,1} & W_{4,2} & v_1 & \epsilon & \dots & . & . & . \\ . & . & . & . & \dots & . & . & . \\ . & . & . & . & \dots & . & . & . \\ . & . & . & . & \dots & \epsilon & v_2 & W_{2N-2,2N} \\ . & . & . & . & \dots & v_2 & \epsilon & v_1 \\ v_2 & . & . & . & \dots & W_{2N,2N-2} & v_1 & \epsilon \end{pmatrix} \quad (4)$$

Here ϵ represents the excitation energy of the Q_y state of an individual BChl and is commonly referred to as site energy. The parameters v_1 and v_2 account for nearest neighbor interactions between chromophores. These interactions as well as the interactions W_{jk} reflect the symmetry of the B850 aggregate, i.e., an 8-fold axis.

In order to determine the parameter C , it suffices to know a single matrix element W_{jk} . In our procedure we define a third parameter $v_3 = W_{13}$ to be adjusted to match the spectrum of excitation energies in ref 56. The constant C in (3), for all further matrix elements, is then given by

$$C = v_3 \left(\frac{\vec{d}_1 \cdot \vec{d}_3}{r_{13}^3} - \frac{3(\vec{r}_{13} \cdot \vec{d}_1)(\vec{r}_{13} \cdot \vec{d}_3)}{r_{13}^5} \right)^{-1} \quad (5)$$

Altogether, four parameters ϵ, v_1, v_2, v_3 establish the complete Hamiltonian in the basis (1). Of these parameters ϵ is trivial in that it solely shifts the spectrum, i.e., replacing $\epsilon \rightarrow \epsilon + \epsilon_1$ shifts the spectrum by ϵ_1 .

Further below we will determine a value for v_3 which results in a C value in (5) of $519\ 310\ \text{\AA}^3\ \text{cm}^{-1}$. This value corresponds to a magnitude of the transition dipole moment of the BChls of about 11 D if one assumes an optical density $n_{\text{opt}} = 1$. We note that the magnitude of this transition dipole moment, derived purely from fitting the exciton band structure of a quantum calculation,⁵⁶ is larger than the previously estimated values of transition dipole moment for BChls in organic solvent; the latter range from 6.1⁵⁷ to 7.7 D.⁵⁸

Figure 6 represents a spectrum of the Hamiltonian for LH-II for typical parameters ϵ, v_1, v_2, v_3 . One can recognize two bands of excitations, a wide band at lower excitation energies and a narrower band at higher excitation energies. Each band consists of a nondegenerate high energy level as well as a nondegenerate low energy level and further states (in the present case six) at intermediate energies that are pairwise degenerate. An occurrence of two such bands is typical for quantum systems of circular geometry with an underlying dimeric structure, i.e., with significant differences in the nearest neighbor couplings v_1 and v_2 . In fact, the gap between the two bands is approximately $2|v_1 - v_2|$ whereas the overall width of both bands is approximately $2v_1 + 2v_2$. In the present case the band at higher energies is narrower due to the dipolar coupling W_{jk} and due to

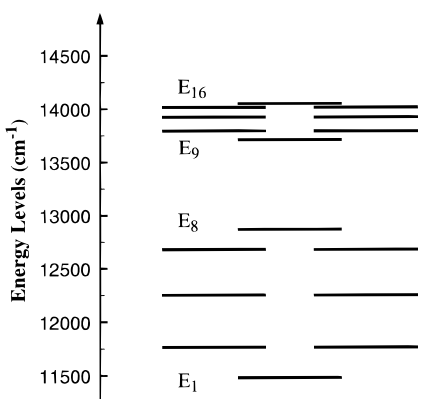


Figure 6. Energies associated with the eigenstates (exciton states) of the effective Hamiltonian describing the aggregate of B850 BChls in LH-II. The ϵ -value was chosen such that energies E_2, E_3 coincide with the spectral maximum of the circular aggregate at 850 nm.

the property $v_1 > 0$ and $v_2 > 0$ assumed in evaluating the spectrum shown in Figure 6.

The main features of the spectrum in Figure 6 can be abstracted from the four nondegenerate levels at energies E_1, E_8, E_9 , and E_{16} (edges of lower energy band) and E_1, E_8, E_9 , and E_{16} (edges of higher energy band). The number of these characteristics coincides with the number of parameters ϵ, v_1, v_2, v_3 that determine the Hamiltonian (4).

Since the spectrum of the B850 BChl system in LH-II, corresponding to the idealized stick spectrum given in Figure 6, is not available through experiments, we resort to results of extensive quantum-chemical calculations reported in ref 56. In these calculations a much larger basis of excitations, e.g., including also Q_x and charge transfer excitations, was employed and a ZINDO semiempirical Hamiltonian⁵⁹ was used. The calculations yielded the following energy levels (in units of cm^{-1})

$$E_1 = 11\,786, \quad E_8 = 13\,166, \quad E_9 = 14\,017, \quad E_{16} = 14\,349 \quad (6)$$

We seek to choose the parameters ϵ, v_1, v_2, v_3 in (4) such that the effective Hamiltonian description yields a spectrum in which the energies E_1, E_8, E_9 , and E_{16} are matched to (6). For this purpose we determine these energy levels for the Hamiltonian (4) in terms of the parameters ϵ, v_1, v_2, v_3 .

Eigenvalue Problem for the Effective Hamiltonian. In case of the B850 system of LH-II the 16-dimensional Hamiltonian (4) can be written in a form that reflects the dimeric structure of the BChl aggregate with C_8 symmetry

$$\hat{H} = \begin{pmatrix} \hat{H}_{11} & \hat{H}_{12} & \cdot & \hat{H}_{18} \\ \hat{H}_{21} & \hat{H}_{22} & \cdot & \hat{H}_{28} \\ \cdot & \cdot \\ \cdot & \cdot \\ \cdot & \cdot \\ \hat{H}_{81} & \hat{H}_{82} & \cdot & \hat{H}_{88} \end{pmatrix} \quad (7)$$

Here the \hat{H}_{jk} are actually 2×2 matrices that can be identified through comparison with (4). One can readily verify, for example,

$$\hat{H}_{11} = \begin{pmatrix} \epsilon & v_1 \\ v_1 & \epsilon \end{pmatrix}, \quad \hat{H}_{12} = \begin{pmatrix} W_{13} & W_{14} \\ W_{22} & W_{24} \end{pmatrix} \quad (8)$$

The C_8 symmetry of the BChl aggregate implies the symmetry property

$$\hat{H}_{jk} = \hat{H}_{j+m, k+m}, \quad m = 1, 2, \dots, 8 \quad (9)$$

The coupling between two BChls (3) is symmetric

$$W_{ij} = W_{ji} \quad (10)$$

This implies the second symmetry property

$$\hat{H}_{ij} = \hat{H}_{ji}^\dagger \quad (11)$$

where the dagger denotes the transpose.

One can generalize the present description to the case of a circular aggregate of $2N$ BChls with an N -fold symmetry, which we will do presently. We will use below cyclic labels such that the index $k = N + 1$ is identified with $k = 1, k = N + 2$ with $k = 2$, etc. The eigenvectors of (7) can be written

$$\begin{aligned} |n, \beta\rangle &= \frac{1}{\sqrt{N}} \sum_{k=1}^N \exp((2ikn\pi)/N) |k, \beta\rangle, \\ |k, \beta\rangle^T &= (0 \dots \underbrace{1 \dots 0}_{\text{kth position}}) v_{k\beta}^T \end{aligned} \quad (12)$$

where we introduced N to count the symmetry of the circular aggregate; in the case of LH-II $N = 8$. n can assume the values $n = 1, 2, \dots, N$. In this notation $v_{k\beta}$ represents a two-dimensional vector to be determined further below; β will be used later to label the two eigenvectors constructed in the corresponding two-dimensional space. The eigenvalue problem is then stated in the form

$$\hat{H} |\overline{n, \beta}\rangle = E_{n, \beta} |\overline{n, \beta}\rangle \quad (13)$$

One can demonstrate that (12), indeed, provides a solution of (13). Assuming orthonormality of the states $|k, \beta\rangle$ one obtains

$$\begin{aligned} \sum_{k=1}^N \hat{H}_{jk} \exp((2in(k-j)\pi)/N) \exp((2inj\pi)/N) v_{n\beta} &= \\ E_{n\beta} \exp((2inj\pi)/N) v_{n\beta} \end{aligned} \quad (14)$$

The reader should note that cyclic labels are employed as explained above. Here $v_{n\beta}$ is a yet unknown, two-dimensional vector. Exploiting the symmetry property (9) one can demonstrate that the two-dimensional matrix

$$\hat{h}_n = \sum_{k=1}^N \hat{H}_{jk} \exp((2in(k-j)\pi)/N) \quad (15)$$

is independent of j such that one can state the eigenvalue problem (14) in the form

$$\hat{h}_n v_{n\beta} = E_{n\beta} v_{n\beta} \quad (16)$$

Solution of this equation leads to the spectrum shown in Figure 6.

In the case of $v_1 > v_2$, for a given n the lower energy eigenvalue, labeled by $\beta = 1$, corresponds to a state in the lower band in Figure 6 and the higher energy eigenvalue, labeled by $\beta = 2$, corresponds to a state in the upper band. One can show that the states corresponding to the nondegenerate energies E_1, E_8, E_9 , and E_{16} are given by the quantum numbers $n = 8, \beta = 1$, by $n = 4, \beta = 1$, by $n = 4, \beta = 2$, and by $n = 8, \beta = 2$, but not necessarily in the same order (the order depends on the signs of v_1 and v_2). For an evaluation of the energies E_1, E_8, E_9 , and

E_{16} one needs to diagonalize the two matrices \hat{h}_4 and \hat{h}_8 given by

$$\begin{aligned}\hat{h}_4 &= \hat{H}_{11} - \hat{H}_{12} + \hat{H}_{13} - \hat{H}_{14} + \hat{H}_{15} - \hat{H}_{16} + \hat{H}_{17} - \hat{H}_{18} \\ \hat{h}_8 &= \hat{H}_{11} + \hat{H}_{12} + \hat{H}_{13} + \hat{H}_{14} + \hat{H}_{15} + \hat{H}_{16} + \hat{H}_{17} + \hat{H}_{18}\end{aligned}\quad (18)$$

The matrix elements of the 2×2 Hamiltonians (17), (18) are expressed in terms of the parameters ϵ , v_1 , v_2 , v_3 as explained above and require a straightforward, albeit numerical, evaluation of the coupling energies (3) based on the coordinates and transition dipole moments as provided in Tables 2–4. The eigenvalue problem associated with (17), (18) can be solved readily, and one obtains

$$\begin{aligned}E_1 &= \epsilon + 1.942v_3 - \sqrt{0.576v_3^2 + (v_1 + v_2 - 0.638v_3)^2} \\ E_8 &= \epsilon - 1.513v_3 - \sqrt{0.089v_3^2 + (v_1 - v_2 + 0.038v_3)^2} \\ E_9 &= \epsilon - 1.513v_3 + \sqrt{0.089v_3^2 + (v_1 - v_2 + 0.038v_3)^2} \\ E_{16} &= \epsilon + 1.942v_3 + \sqrt{0.576v_3^2 + (v_1 + v_2 - 0.638v_3)^2}\end{aligned}\quad (19)$$

We emphasize that the numerical coefficients appearing here stem from a numerical evaluation of the coupling energies W_{jk} according to (3) and Tables 2–4; they are not the result of an analytical theory.

Equating the energies in (19) with the values in (6) leads to $\epsilon = 13\ 362\text{ cm}^{-1}$, $v_1 = 806\text{ cm}^{-1}$, $v_2 = 377\text{ cm}^{-1}$, and $v_3 = -152\text{ cm}^{-1}$. The two degenerate states with energies E_2 , E_3 are the only allowed states as shown below. Accordingly, the energies E_2 , E_3 should coincide with the spectral maximum of the circular BChls aggregate, namely, 850 nm. This requires one to shift the corresponding value of ϵ to $\epsilon = 13\ 059\text{ cm}^{-1}$, which implies that the individual BChls in LH-II have absorption maxima at 766 nm. It is intriguing that this site energy of 766 nm is nearly the same as the absorption maximum (772 nm) of BChl-a in organic solvent.⁶⁰ The energy spectrum shown in Figure 6 corresponds, in fact, to an effective Hamiltonian with the parameters just determined. The states corresponding to the spectrum are referred to as excitons.

It should be noted that our calculated exciton level spacing in the lower exciton band is in good agreement with recent hole-burning experiments of Wu et al. in which a 870 nm shoulder was observed at the red edge of the 850 nm band of the B850 BChls and was assigned to the lowest exciton level (E_1 in Figure 6) of the aggregate.⁶¹ In accordance with our calculation, this lowest exciton level was observed to lie 200 cm⁻¹ below the two optically allowed levels (E_2 and E_3 in Figure 6) that give rise to the B850 band maximum.

The Hamiltonian (4) can be extended in an obvious way to describe several rings of LH-II and also to describe LH-I. In the latter case we will assume that the same nearest neighbor matrix elements v_1 and v_2 apply since LH-I also exhibits a circular aggregate of BChl dimers and since the nearest neighbor distances in LH-I are similar to those in LH-II (see above). The scaling factor for the dipolar coupling, v_3 , is transferable. However, the site energy ϵ for LH-I may differ from that of LH-II due to a different environment of the BChls.

Applying the calculations with unaltered parameters v_1 , v_2 , and v_3 to LH-I, i.e., setting $N = 16$, yields a spectrum similar to that shown in Figure 6, albeit with 16 states forming the lower band and 16 states forming the upper band. The states

TABLE 1: Oscillator Strengths and Energies (in cm⁻¹) for the Exciton States of the B-850 BChls in LH-II and of the B875 BChls in LH-I^a

LH-II	f_n	E_n	LH-I	f_n	E_n
1	0.000	11 482	1	0.019	11 335
2	7.869	11 765	2	15.714	11 429
		(850 nm)			(875 nm)
3	7.869	11 765	3	15.714	11 429
14	0.003	14 012	30	0.036	13 893
15	0.003	14 012	31	0.036	13 893
16	0.256	14 046	32	0.480	13 902
Σ	16.000		Σ	32.000	

^a The values are obtained from the effective Hamiltonian calculation. In LH-II only the two degenerate states at 850 nm carry significant oscillator strength. The lowest energy exciton state is optically forbidden. In LH-I the two degenerate states at 875 nm carry the main part of the oscillator strength, while the lowest energy exciton state is weakly allowed.

with energies E_2 , E_3 are again the only optically allowed states and therefore are assigned to the observed spectral maximum of 875 nm. This implies that an ϵ of 12 911 cm⁻¹ must be chosen for LH-I. The key excitations determined for the B850 system in LH-II and for the B875 system in LH-I are characterized in Table 1.

Optical Properties. A key function of the BChl aggregate in the light-harvesting complexes is optical absorption. Naturally, the optical absorption characteristics of the exciton states should be characterized. For this purpose we note that the $2N$ excitations can be expressed through the single excitations of individual BChls (1) as follows

$$|\tilde{n}\rangle = \sum_{\alpha=1}^N C_{n\alpha} |\alpha\rangle, \quad n = 1, \dots, 2N \quad (20)$$

where $C_{n\alpha}$ are complex coefficients that can be evaluated according to the scheme presented above. The transition dipole moment f_n connected with the single photon excitations of the exciton state $|\tilde{n}\rangle$ is

$$\vec{f}_n = \sum_{\alpha=1}^N C_{n\alpha} \vec{D}_{\alpha} \quad (21)$$

where \vec{D}_{α} is the transition dipole moment for the Q_y transition of BChl α . The oscillator strength associated with the transition to the state $|\tilde{n}\rangle$ is $|\vec{f}_n|^2$.

The exciton states can be assumed to be orthonormal, i.e.,

$$\langle \tilde{n} | \tilde{m} \rangle = \delta_{nm} \quad (22)$$

From this property follows, using (2) and (20),

$$\sum_{n=1}^{2N} C_{n\alpha}^* C_{n\alpha'} = \delta_{\alpha\alpha'} \quad (23)$$

One can derive then readily the oscillator strength sum rule

$$\sum_{n=1}^{2N} |\vec{f}_n|^2 = \sum_{\alpha=1}^{2N} |\vec{D}_{\alpha}|^2 = 2N S_y \quad (24)$$

where the second equality follows from the fact that all BChls carry identical oscillator strengths $|\vec{D}_{\alpha}|^2 = S_y$. The sum rule (24) implies that the sum of the oscillator strengths of all exciton states $|\tilde{n}\rangle$ is equal to $2N$ times the oscillator strength of the Q_y transition of the individual BChls. This rule applies, irrespective of the circular symmetry of the system. In the case of an uncoupled system each BChl carries the same oscillator strength; however, in the case of coupled BChls, as described by the effective Hamiltonian (4), the resulting exciton states do not

share the oscillator strength equally; rather, in the case of perfect C_N symmetry, the two states with (degenerate) energies E_2 and E_3 carry all the oscillator strength, each an oscillator strength of N times S_y . If the wave functions are chosen to be real and orthonormal, the transition dipole moments of the states are orthogonal to each other. Table 1 lists the oscillator strengths and energies for the states of an LH-II aggregate and an LH-I aggregate, respectively. Only the state of lowest energy and the states with energy E_2, E_3 , i.e., the states that carry oscillator strengths, are listed. This result shows that the latter energies must coincide with the 850 nm absorption maximum as surmised above.

In case of LH-I, the state of lowest energy carries weak, but not vanishing, oscillator strength as presented in Table 1. This residual oscillator strength stems from an orientation of the BChls that endows each D_α with a small component normal to the plane of the ring. The corresponding orientation of the BChls may reflect an error in the predicted structure of LH-I. However, it is also possible that in the photosynthetic apparatus BChl orientations may be systematically altered as to endow the light-harvesting complexes with transition dipole moments in the direction normal to the membrane (i.e., ring) plane such that light can be re-emitted, e.g., under strong light conditions, providing, thereby, a mechanism to avoid heating of the PSU under intense light conditions. However, annihilation processes or nonradiative decay may also be instrumental in this regard.

From the results in Table 1 emerges a remarkable conclusion regarding the circular architecture of light-harvesting complexes: the circular symmetry, together with the dipolar coupling, concentrates all oscillator strength into two isoenergetic states absorbing perpendicular to each other in the plane of the membrane; the exciton state of lowest energy does not carry any oscillator strength such that this state conserves the light energy, rather than re-emitting the light. The circular BChl system absorbs energy, either directly or indirectly through intracomplex excitation transfer, into the states of energy E_2, E_3 and relaxes rapidly to the lowest energy state. At room temperature ($T = 300$ K) the two absorbing degenerate states, as evaluated by means of the effective Hamiltonian, in LH-II lie $1.36 k_B T$ above the lowest excited state. The two optically allowed excitons will then remain together 33% populated after thermal relaxation.

The same argument applies for an LH-I aggregate. Here, the difference between the lowest exciton state at E_1 and the two degenerate states at E_2 and E_3 is, however, only $0.45 k_B T$ such that the two optically allowed exciton states remain 42% populated in LH-I. Again, the lowest exciton state is optically forbidden and can thus store the energy until it is transferred to the RC. Remarkably, the more complete quantum-chemical calculation in ref 56 places the lowest state for a 16-BChl system actually about $3k_B T$ below the optically allowed states. This increased stabilization, mainly due to interaction with higher energy charge transfer excitations not included in the effective Hamiltonian description, results in only a 9% occupancy of the two optically allowed exciton states. One can expect a similar stabilization of the lowest energy exciton state in case of the LH-I ring system such that the occupancy of the optically allowed exciton states would be reduced as well. It is obviously of great interest to know the exact difference of E_1 and E_2, E_3 in the LH-II and LH-I exciton systems and to understand the mechanism for stabilizing the lowest energy exciton.

The presented scenario assumes perfect circular symmetry. Vibrational motion of the protein and the BChls broadens the spectrum and affects the exciton states. Likewise, an indigenous, glasslike disorder of the protein will induce differences

in the local excitation energies of the BChls. The question arises as to how far the presented scenario remains valid for a disordered aggregate, i.e., how far oscillator strength concentrates in the states with energy $E_{2,3}$ and the lowest energy exciton state remains forbidden. In order to answer this question at least partially, we will consider the effect of static, inhomogeneous broadening on the level ordering and oscillator strength distribution of the LH-II exciton system.

The Effect of Diagonal Disorder. In this section we consider the ring of B850 BChls in LH-II. We will assume that the centers and orientations of the BChls obey the exact C_8 symmetry, such that the off-diagonal elements of the effective Hamiltonian do not alter their values, but that the diagonal matrix elements exhibit an inhomogeneous broadening. The latter is described through a Gaussian distribution of the excitation energies ϵ_α of the individual BChls

$$p(\epsilon_\alpha) = \frac{1}{\sqrt{2\pi}\sigma} \exp [-(\epsilon_\alpha - \epsilon)^2/2\sigma^2] \quad (25)$$

The inhomogeneous broadening can be treated as static since the frequency of the light absorbed exceeds the relaxation rates governing the inhomogeneous broadening by orders of magnitude. The width σ should account for the observed spectral inhomogeneities from hole-burning experiments. A similar approach to describe inhomogeneous broadening of BChl aggregates has been carried out recently in ref 62.

A numerical description of the disordered aggregate is straightforward. We generated, by means of a random number generator, an ensemble of 1000 aggregates, each characterized through a particular set of energies ($\epsilon_1, \epsilon_2, \dots, \epsilon_{16}$). We then diagonalized the resulting Hamiltonians for each such aggregate and determined the average excitation energies as well as the average oscillator strengths for all exciton states. We carried out such calculation for σ -values ranging from 0 to 1500 cm^{-1} in steps of 5 cm^{-1} . The resulting energies and oscillator strengths are provided in Figure 7. Figure 7a shows a splitting of the degenerate energy levels (e.g., E_2, E_3) with increasing σ and a widening of the exciton bands. Most interesting is the redistribution of oscillator strengths among the excitonic states with increasing diagonal disorder shown in Figure 7b: the allowed states of energy E_2, E_3 lose oscillator strength, a major part of which shifts to the lowest energy exciton state. However, this effect develops significantly only for $\sigma \geq 170 \text{ cm}^{-1}$ for which the oscillator strengths of states of energy E_1 and $E_{2,3}$ are larger than 0.3 and less than 7.6, respectively (in units of S_y). This implies that disorder corresponding to σ -values of less than about 170 cm^{-1} does not affect significantly the characteristics of the exciton states relevant for light absorption and for conservation of light energy in the lowest exciton state. The oscillator strengths of the strongly allowed exciton states can be considered a qualitative measure of the delocalization of the exciton states in LH-II. Noticing the sum rule (24), which applies also to the disordered system, one notes that the complete ordered system with coherent exciton states extended over the complete LH-II ring shifts the oscillator strengths (for the Q_y transition) S_y of the 16 BChls into two states, each with oscillator strength of $8S_y$. A decrease of the oscillator strength of these states below this value implies an imperfect delocalization. Indeed, this theoretically predicted enhancement of the transition dipole strength has been observed in recent measurements of the nonlinear absorption and of the differential optical density spectrum of LH-II from *Rb. sphaeroides*,⁶³ which indicates exciton delocalization over the entire circular aggregate of B850 BChls. Exciton delocalization is also consistent with the

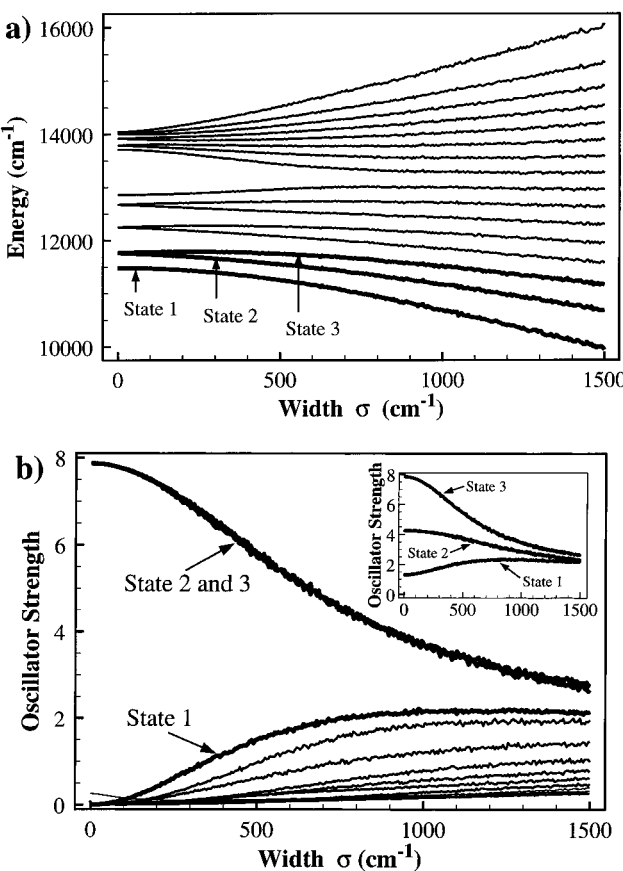


Figure 7. (a) Energy levels of the aggregate of the 16 B850 BChls in LH-II with diagonal disorder. The diagonal elements of the Hamiltonian are distributed according to a Gaussian distribution with varying width σ . Energies shown are averaged over an ensemble of 1000 aggregates for each σ -value. (b) Oscillator strength (in units S_y ; see text) of the excitonic states corresponding to the energy levels in (a) for the same average over 1000 aggregates. The oscillator strength of excitons at energies E_1 , E_2 , E_3 are highlighted. The inset shows the corresponding oscillator strength of the excitons at the lowest three energies for the aggregate as in (a), except that an $\alpha\beta$ -heterodimer had been eliminated such that the disordered aggregates contain 14 BChls. ($\epsilon = 13\,059\text{ cm}^{-1}$, $v_1 = 806\text{ cm}^{-1}$, $v_2 = 377\text{ cm}^{-1}$, and $v_3 = -152\text{ cm}^{-1}$.) The geometry of the aggregate is provided in Table 2.

observed larger relative bleaching for the B850 BChls aggregate of LH-II in pump–probe experiments.⁴¹

The inset in Figure 7b demonstrates that disruption of the circular arrangement of the BChls, in addition to diagonal disorder, has a more pronounced effect on the pattern of oscillator strengths. If one eliminates one pair of BChls, corresponding to the elimination of an $\alpha\beta$ -heterodimer of LH-II, the oscillator strength of the lowest energy state jumps for $\sigma = 0$ to about 1 and the oscillator strength of one of the strongly absorbing states decreases to about 5 (in units of S_y). One can conclude from this finding that disrupting the LH-II rings should be avoided at low light intensities, when light energy needs to be conserved, as long as a small oscillator strength of the lowest exciton states, as suggested, is a determinant factor for the efficiency of the light-harvesting system. However, such disruption may occur in the LH-I complex which has been postulated to actually form under certain conditions an open ring through the action of Puf X; the opening of the LH-I ring may facilitate unbinding and rebinding of quinone to the RC.

The question arises how large the diagonal disorder in LH-II may actually be. To answer this we have determined the spectrum of the disordered BChl aggregate for a disorder characterized through $\sigma = 170\text{ cm}^{-1}$. For this purpose we

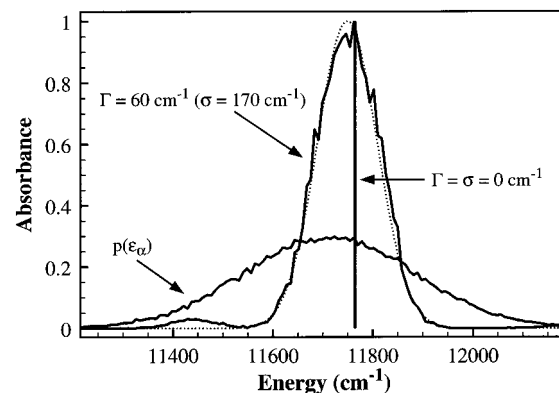


Figure 8. Absorbance of a disordered aggregate of B850 BChls of LH-II. The system corresponds to those in Figure 7 for $\sigma = 170\text{ cm}^{-1}$, albeit with a sample size of 5000. The construction of the absorbance shown is explained in the text. The calculated absorbance is well approximated by a Gaussian with the width of 60 cm^{-1} (dotted line). The figure presents also the absorbance for $\sigma = 0$ (single stick) as well as the distribution $p(\epsilon_\alpha)$ of ϵ_α -values assumed.

considered an ensemble of 5000 aggregates with randomly selected diagonal matrix elements in the effective Hamiltonian. The energies and oscillator strengths of all exciton states were evaluated and collected into bins of width 5 cm^{-1} along the energy axis. Figure 8 shows the resulting average spectrum of nearly Gaussian shape with a width of $\Gamma = 60\text{ cm}^{-1}$. As a reference the spectrum for a completely ordered aggregate (all diagonal elements ϵ_α equal $13\,059\text{ cm}^{-1}$) is also shown as well as the distribution of ϵ_α . One can recognize that the spectrum of the ensemble is narrowed relative to the distribution of ϵ_α by a factor of 2.8. This feature, referred to as exchange narrowing,⁶⁴ is well-known and the factor observed agrees well with the theoretical value \sqrt{N} , where N denotes the symmetry of the aggregate and assumes the value $N = 8$.

Hole-burning spectroscopy⁶⁵ has provided estimates for the inhomogeneous broadening of the B850 BChl system in LH-II; LH-II of *Rb. sphaeroides* exhibits a width of 60 cm^{-1} . According to Figure 8 this would correspond to a diagonal disorder of $\sigma = 170\text{ cm}^{-1}$. As judged from the results in Figure 7, such disorder produces a recognizable, albeit small effect on the oscillator strengths of the exciton states in the LH-II B850 BChl aggregate such that the functional implications of the exciton structure, spelled out above, hold true even if inhomogeneous broadening is taken into account. This conclusion is corroborated by the measurements reported in both refs 63 and 41, which attribute to the B850 BChl optical absorption an oscillator strength several times that of a BChl monomer.

Intercomplex Excitation Transfer. The transfer of electronic excitation, after BChl systems have relaxed to the lowest excited state of LH-II and until the arrival of the excitation in the RC, involves three steps: (i) transfer of the electronic excitation between two LH-II rings (in case that light is initially absorbed by an LH-II ring not in direct contact with LH-I; see Figure 2a); (ii) transfer of the electronic excitation from LH-II to LH-I; (iii) transfer of the electronic excitation from LH-I to the RC. All three transfers require that the initial and final states are in resonance, i.e., that $|E_{\text{initial}} - E_{\text{final}}|$ is of the order of the coupling energy or less; the coupling energies, as estimated from the transfer rates of $0.1\text{--}1\text{ ps}^{-1}$, assume values in the range of 1 cm^{-1} . The final state in the transfer processes can be any exciton state; however, due to thermal relaxation, the initial state is most likely the lowest energy exciton state as argued above. The crucial question arises then if the lowest energy exciton state, though optically forbidden, can be an effective participant in the transfers (i, ii, iii).

TABLE 2: Structural Data for the LH-II Aggregates: Coordinates (x , y , z) and Dipole Moments (Unit Vectors Only) of the Bacteriochlorophylls Used in the Effective Hamiltonian Calculations^a

LH-II-1	x	y	ϕ	LH-II-2	x	y	ϕ
1	102.451	-20.436	3.289	1	132.644	32.942	2.791
2	110.250	-15.464	0.361	2	141.870	33.590	6.147
3	113.987	-7.414	4.074	3	148.995	38.882	3.577
4	115.986	1.616	1.146	4	155.061	45.864	0.649
5	112.936	9.951	4.860	5	156.358	54.644	4.362
6	107.964	17.750	1.932	6	155.710	63.870	1.434
7	99.914	21.487	5.645	7	150.418	70.995	5.148
8	90.884	23.486	2.717	8	143.436	77.061	2.220
9	82.549	20.436	0.147	9	134.656	78.358	5.933
10	74.750	15.464	3.503	10	125.430	77.710	3.005
11	71.013	7.414	0.933	11	118.305	72.418	0.435
12	69.014	-1.616	4.288	12	112.239	65.436	3.791
13	72.064	-9.951	1.718	13	110.942	56.656	1.221
14	77.036	-17.750	5.073	14	111.590	47.430	4.576
15	85.086	-21.487	2.504	15	116.882	40.305	2.006
16	94.116	-23.486	5.859	16	123.864	34.239	5.361

LH-II-1	z	θ	LH-II-2	z	θ
1	72.225	-0.126	1	72.225	-0.126
2	72.084	-0.128	2	72.084	-0.128

^a Since every second bacteriochlorophyll is located at the same z -coordinate, we give this coordinate only for the first two bacteriochlorophylls of each ring. The dipole moment unit vectors are defined through angles ϕ (azimuthal angle) and θ (angle with respect to the z -axis).

In order to answer the stated question, we will extend the effective Hamiltonian description of intracomplex states to encompass two LH-II units, an LH-II together with an LH-I unit and LH-I together with the relevant RC BChl components. The intercomplex excitation transfer relies in this description on the coupling matrix elements (3), (5); no further mechanisms are needed to explain the transfer processes (i, ii, iii). We will assume in our description the same parameters ϵ , v_1 , v_2 , v_3 as in the previous description, except where stated otherwise.

Excitation Transfer LH-II \rightarrow LH-II. In order to describe the transfer LH-II \rightarrow LH-II, we need to construct the associated effective Hamiltonian (4) for a system of two LH-II rings. The needed coordinates and transition dipole moments of the individual BChls for the two rings are provided in Table 2. The resulting Hamiltonian matrix is of dimension 32 and can be decomposed into four 16-dimensional submatrices as follows

$$\hat{H} = \begin{pmatrix} \hat{R}_{11} & \hat{R}_{12} \\ \hat{R}_{21} & \hat{R}_{22} \end{pmatrix} \quad (26)$$

where \hat{R}_{11} , \hat{R}_{22} are the effective Hamiltonians for the two rings and \hat{R}_{12} , \hat{R}_{21} describe the coupling between the rings, involving solely dipole-dipole interaction terms (3), (5), i.e., $\hat{R}_{12}(i,j) = W_{i,j}$ where $i = 1, \dots, 16$ is the index of a BChl of the first ring and $j = 1, \dots, 16$ is an index of a BChl of the second ring. One can readily verify the property $R_{12} = \hat{R}_{21}^T$.

Since the reference states for the transfer process (i) defined above are exciton states of the individual LH-II rings, we choose a description in terms of both individual ring excitons as well as in terms of excitons of the LH-II + LH-II two ring system. Accordingly, we determine first the eigenvectors of \hat{R}_{11} and \hat{R}_{22} denoted by $|\omega_n^1\rangle$, $|\omega_n^2\rangle$, where $n = 1, \dots, 16$, and the indices 1, 2 denote the rings, as well as the eigenvalues and eigenvectors λ_n , $|\Omega_n\rangle$ of the two-ring Hamiltonian \hat{H} . For a unified description we extend the dimension of $|\omega_n^1\rangle$ and $|\omega_n^2\rangle$ from 16 to 32 by adding extra zeroes so that the scalar product $\langle \omega_k^1 | \Omega_n \rangle$ denotes the projection of the n th eigenstate of the two-

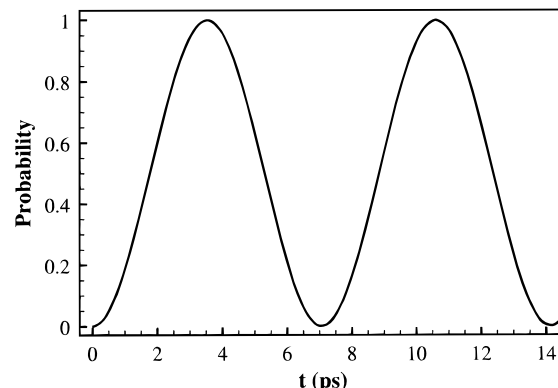


Figure 9. Probability $P(t)$ for LH-II(i) \rightarrow LH-II(ii) excitation transfer evaluated as described in the text. The system is initially in the lowest energy exciton state of LH-II(i). $P(t)$ measures the probability that LH-II(ii) is excited in any of its exciton states. The calculations are based on a 32-dimensional effective Hamiltonian of LH-II(i)+LH-II(ii) with parameters $\epsilon = 13.059 \text{ cm}^{-1}$, $v_1 = 806 \text{ cm}^{-1}$, $v_2 = 377 \text{ cm}^{-1}$, and $v_3 = -152 \text{ cm}^{-1}$. The geometry of the 16 BChls in LH-II(i) is given in Table 2.

ring Hamiltonian \hat{H} onto the k th eigenstate of the respective one-ring Hamiltonian.

The time evolution of an initial state $|\psi(0)\rangle$ can be expressed

$$|\psi(t)\rangle = \sum_n^{4N} |\Omega_n\rangle \langle \Omega_n | \psi(0) \rangle \exp(-i\lambda_n t/\hbar) \quad (27)$$

To describe the LH-II \rightarrow LH-II transfer we choose $|\psi(0)\rangle = |\omega_1^1\rangle$. The probability $P(t)$ of finding the excitation at the second ring, at time t , is

$$P(t) = \sum_n^{2N} P_n(t), \quad P_n(t) = |\langle \omega_n^2 | \psi(t) \rangle|^2 \quad (28)$$

where P_n accounts for the probability that the n th exciton state in ring 2 is populated. Due to the resonance condition, only the lowest exciton state bears a significant occupancy and $P(t)$ exhibits the typical behavior of a pure two-state system

$$P(t) = \sin^2(\pi t/\tau) \quad (29)$$

as shown in Figure 9. One can identify from the numerical results $\tau = 7.08 \text{ ps}$.

The result shown in Figure 9 can be reproduced by considering the pure two-state system $\{|\omega_1^1\rangle, |\omega_1^2\rangle\}$ governed by the Hamiltonian

$$\begin{pmatrix} \langle \omega_1^1 | \hat{H} | \omega_1^1 \rangle & \langle \omega_1^2 | \hat{H} | \omega_1^1 \rangle \\ \langle \omega_1^1 | \hat{H} | \omega_1^2 \rangle & \langle \omega_1^2 | \hat{H} | \omega_1^2 \rangle \end{pmatrix} \quad (30)$$

Since $\langle \omega_1^1 | \hat{H} | \omega_1^1 \rangle = \langle \omega_1^2 | \hat{H} | \omega_1^2 \rangle$, the probability to find the system in state $|\omega_1^2\rangle$, when it has been initially ($t = 0$) in state $|\omega_1^1\rangle$, is

$$P(t) = \sin^2(\langle \omega_1^2 | \hat{H} | \omega_1^1 \rangle t/\hbar) \quad (31)$$

We determined $\langle \omega_1^2 | \hat{H} | \omega_1^1 \rangle = 2.33 \text{ cm}^{-1}$, which corresponds to a period $\tau = 7.17 \text{ ps}$ which, indeed, is close to that reflected in the results shown in Figure 9.

Excitation Transfer LH-II \rightarrow LH-I. An analogous procedure can be applied for the transfer LH-II \rightarrow LH-I combining, in an effective Hamiltonian description, the 16 BChl ring of LH-II with the 32-BChl ring of LH-I. The resulting Hamiltonian matrix \hat{H} can be written again in the form (26) with \hat{R}_{11} representing the LH-II ring through a 16-dimensional matrix, \hat{R}_{22} representing the LH-I ring through a 32-dimensional matrix,

TABLE 3: Structural Data for the LH-I Aggregate^a

LH-I	<i>x</i>	<i>y</i>	ϕ	LH-I	<i>x</i>	<i>y</i>	ϕ
1	44.706	-12.591	4.017	17	-44.706	12.591	0.875
2	47.167	-3.677	1.099	18	-47.167	3.677	4.240
3	46.121	5.476	4.410	19	-46.121	-5.476	1.268
4	44.984	14.653	1.492	20	-44.984	-14.653	4.633
5	40.515	22.709	4.802	21	-40.515	-22.709	1.661
6	35.952	30.752	1.884	22	-35.952	-30.752	5.026
7	28.741	36.485	5.195	23	-28.741	-36.485	2.054
8	21.447	42.169	2.277	24	-21.447	-42.169	5.419
9	12.591	44.706	5.588	25	-12.591	-44.706	2.446
10	3.677	47.167	2.670	26	-3.677	-47.167	5.811
11	-5.476	46.121	5.981	27	5.476	-46.121	2.839
12	-14.653	44.984	3.062	28	14.653	-44.984	6.204
13	-22.709	40.515	0.090	29	22.709	-40.515	3.232
14	-30.752	35.952	3.455	30	30.752	-35.952	0.314
15	-36.485	28.741	0.483	31	36.485	-28.741	3.624
16	-42.169	21.447	3.848	32	42.169	-21.447	0.706
LH-I	<i>z</i>	θ	LH-I	<i>z</i>	θ		
1	71.986	-0.147	1	71.986	-0.147		
2	72.184	-0.098	2	72.184	-0.098		

^a The entries are defined as in Table 2.

and $\hat{R}_{12} = \hat{R}_{21}^T$ representing the intercomplex coupling through a 16×32 matrix containing solely matrix elements (3), (5). Both effective Hamiltonians \hat{R}_{11} and \hat{R}_{22} are set up with the parameters ϵ , v_1 , v_2 , v_3 from the previous sections. The positions and the transition dipole moments of the individual rings are given in Tables 2 and 3.

Inspection of Table 1 shows that the doubly degenerate energy absorbing LH-I exciton states lies closest to the lowest energy of the LH-II exciton. The difference in energies is 53 cm^{-1} in comparison to 147 cm^{-1} between the lowest energy excitons of LH-II and LH-I, which lie next closest. One can expect, therefore, that in the LH-II \rightarrow LH-I transfer the final state is actually one of the two strongly absorbing LH-I exciton states. The corresponding matrix elements $\langle \omega_1^1 | \hat{H} | \omega_2^2 \rangle$ and $\langle \omega_1^1 | \hat{H} | \omega_3^2 \rangle$ are 5.019 and 0.078 cm^{-1} , respectively. Since the states $|\omega_2^2\rangle$ and $|\omega_3^2\rangle$ are energetically degenerate, any linear combination of the states is also a proper exciton state and can serve as the final state. The state given by the linear combination $\gamma_2 |\omega_2^2\rangle + \gamma_3 |\omega_3^2\rangle$ experiences a coupling to the LH-II exciton of $\gamma_2 \langle \omega_1^1 | \hat{H} | \omega_2^2 \rangle + \gamma_3 \langle \omega_1^1 | \hat{H} | \omega_3^2 \rangle$. Excitation transfer will select that linear combination as a final state that bears the largest matrix element, in the present case $(5.019^2 + 0.078^2)^{1/2} \text{ cm}^{-1} = 5.02 \text{ cm}^{-1}$. This matrix element corresponds to $\tau \approx 3.3 \text{ ps}$, which is in agreement with the observed transfer time.⁴⁰

LH-I \rightarrow RC Transfer. We consider now the transfer from LH-I to the RC. Building on the previous examples, we include in our present description solely the lowest energy exciton state of LH-I, denoted by $|1\rangle$. We then consider two basis sets to describe the transfer. One basis set includes the Q_y excitations of the two BChls forming the so-called special pair of the RC; the respective states are denoted by $|2\rangle$ and $|3\rangle$. The corresponding Hamiltonian is

$$\hat{H}_1 = \begin{pmatrix} \epsilon_1 & v_{12} & v_{13} \\ v_{12} & \epsilon_2 & v_{sp} \\ v_{13} & v_{sp} & \epsilon_2 \end{pmatrix} \quad (32)$$

Here v_{sp} describes the coupling between the BChls of the special pair and is taken to be $v_{sp} = 1000 \text{ cm}^{-1}$ in accordance with the value suggested in ref 66. ϵ_1 is the energy of the LH-I lowest energy exciton state, chosen here as $11\,335 \text{ cm}^{-1}$ in accordance with Table 1. ϵ_2 is chosen to place the lowest state of the special pair with energy $\epsilon_2 - v_{sp}$ at the experimentally determined value

TABLE 4: Structural Data for the Accessory Bacteriochlorophylls and the Special Pair in the Photosynthetic Reaction Center^a

Chl	<i>x</i>	<i>y</i>	ϕ	<i>z</i>	θ
AC[1]	-2.852	10.539	1.239	70.886	0.402
AC[2]	3.369	-9.909	4.474	72.059	0.496
SP[1]	-3.402	-2.049	1.156	68.512	0.349
SP[2]	3.317	2.301	4.310	68.262	0.327

^a The entries are defined as in Table 2.

of 865 nm , i.e., $\epsilon_2 = 12\,560 \text{ cm}^{-1}$. The matrix elements v_{12} and v_{13} describe the coupling of the LH-I exciton state to the special pair BChls. Using the expressions (3), (5) for $v_3 = -152 \text{ cm}^{-1}$, as determined above, and employing the appropriate wave function of the lowest energy exciton state yield $v_{12} = 0.46 \text{ cm}^{-1}$ and $v_{13} = 0.50 \text{ cm}^{-1}$, the close values reflecting the symmetry of the LH-I-RC complex.

In a second description we include, besides the mentioned states $|1\rangle$, $|2\rangle$, $|3\rangle$, also states $|4\rangle$, $|5\rangle$, which account for the Q_y excitations of the two so-called accessory BChls in the RC. The corresponding Hamiltonian is

$$\hat{H}_2 = \begin{pmatrix} \epsilon_1 & v_{12} & v_{13} & v_{14} & v_{15} \\ v_{12} & \epsilon_2 & v_{sp} & W_{24} & W_{25} \\ v_{13} & v_{sp} & \epsilon_2 & W_{34} & W_{35} \\ v_{14} & W_{24} & W_{34} & \epsilon_3 & W_{45} \\ v_{15} & W_{25} & W_{35} & W_{45} & \epsilon_3 \end{pmatrix} \quad (33)$$

Here we introduced a new parameter ϵ_3 to describe the local excitation energies of the two accessory BChls and added dipolar couplings W_{jk} evaluated according to (3), (5) as well as matrix elements v_{14} , v_{15} evaluated in analogy to v_{12} and v_{13} as explained above. The BChl coordinates and dipole moments needed for the evaluation of matrix elements in (32), (33) are provided in Table 4. Due to the coupling with the accessory BChls we have to choose $\epsilon_2 = 12\,748 \text{ cm}^{-1}$ in order to place the lowest state of the special pair at 865 nm . For ϵ_3 we choose a value $12\,338 \text{ cm}^{-1}$, which places the optically allowed transition of the accessory BChls at 802 nm .

It is of interest to examine the actual numerical values of the elements of the effective Hamiltonians below (in units of cm^{-1})

$$\hat{H}_1 = \begin{pmatrix} 11335 & 0.46 & 0.50 \\ & 12560 & 1000 \\ & & 12560 \end{pmatrix}$$

$$\hat{H}_2 = \begin{pmatrix} 11335 & -0.46 & -0.50 & 3.4 & 2.6 \\ & 12748 & 1000 & -396 & -51 \\ & & 12748 & -27 & -418 \\ & & & 12338 & 57 \\ & & & & 12338 \end{pmatrix} \quad (34)$$

One can recognize that the matrix elements describing the coupling between the LH-I exciton state $|1\rangle$ and the RC BChl excitations are small compared to the intra-RC couplings. As a result one can consider first the eigenstates of the intra-RC Hamiltonians, i.e., of

$$\begin{pmatrix} \epsilon_2 & v_{sp} & W_{24} & W_{25} \\ v_{sp} & \epsilon_2 & W_{34} & W_{35} \\ W_{24} & W_{34} & \epsilon_3 & W_{45} \\ W_{25} & W_{35} & W_{45} & \epsilon_3 \end{pmatrix} \quad (35)$$

and then determine the coupling of the respective states with the LH-I exciton state. It is also of interest to note that the coupling of the LH-I exciton state to the accessory BChls is stronger by almost an order of magnitude than the coupling to the special pair BChls.

The diagonal elements of the Hamiltonians in (34), (35) have been chosen to match the absorption maxima at 865 and 802 nm attributed to special pair and accessory BChls but not to ascertain resonance of any of the RC states with one of the exciton states of LH-I. Such resonance can be achieved by shifting the value of ϵ_1 , the first diagonal entry in (34) describing the lowest energy LH-I excitation. In the following we determine the eigenstates of (35) and the couplings to LH-I exciton states. Exciton transfer times refer then always to resonant situations; i.e., it is assumed that the RC and LH-I energies are optimally matched for the respective transfers to take place. This correction of the energy is crucial to obtain excitation transfer, the latter requiring a matching of energies with a precision of about 1 cm^{-1} . The occurrence of excitation transfer implies that resonance is achieved under native conditions, for which purpose vibrations coupled to the optical transitions and local electrostatic energies are almost likely exploited.

In the case that one neglects the existence of the accessory BChls; i.e., for the effective Hamiltonian (32), one finds that the lower energy state of the special pair exhibits a coupling $V = 0.028\text{ cm}^{-1}$ to the state $|1\rangle$. This coupling corresponds to a transition time $\tau = 595\text{ ps}$ for perfect resonance. This time is much longer than the observed transfer time of about 35 ps.⁶⁷

In the case that one includes the accessory BChl in the description one determines the RC exciton states at energies $E_1 = 11\,560\text{ cm}^{-1}$, $E_2 = 12\,260\text{ cm}^{-1}$, $E_3 = 12\,469\text{ cm}^{-1}$, $E_4 = 13\,882\text{ cm}^{-1}$ with the associated eigenvectors

$$v_1 = \begin{pmatrix} 0.63 \\ -0.63 \\ 0.32 \\ -0.32 \end{pmatrix}, \quad v_2 = \begin{pmatrix} -0.21 \\ -0.19 \\ -0.66 \\ -0.70 \end{pmatrix}, \quad v_3 = \begin{pmatrix} 0.32 \\ -0.32 \\ -0.65 \\ 0.61 \end{pmatrix}, \\ v_4 = \begin{pmatrix} -0.68 \\ -0.68 \\ 0.19 \\ 0.21 \end{pmatrix} \quad (36)$$

The couplings to the LH-I exciton states are 0.26, 3.9, 0.59, and 1.9 cm^{-1} . The first state corresponds to the lowest special pair excitation, with a significant admixture of accessory BChl excitations as described by the Hamiltonian (35). Due to these admixtures, the coupling of this state to the LH-I state is significantly stronger than for the pure special pair state. In fact, the stated coupling energy corresponds to a transfer time of $\tau = 65\text{ ps}$. This time scale is about two times longer than that expected from observations.⁶⁷ The predicted time scale depends sensitively on the matrix elements describing the RC BChls in (35), in particular on $\epsilon_3 - \epsilon_2$ and on W_{34} , and can readily shorten by a factor of 2 through lower values of $\epsilon_3 - \epsilon_2$ and higher values of W_{34} . The resonance condition places the lowest energy excitation of LH-I at $11\,560\text{ cm}^{-1}$, which is 225 cm^{-1} above the value in Table 1. Such deviation could readily be attributed to vibrational coupling or a shift of the site energy.

It is of interest to consider the coupling of the RC states in (36) to the LH-I excitons at E_2 , E_3 . One determines the values 40, 0.10, 15, and 0.06 cm^{-1} (E_2 state) and 17, 1.7, 3.2, and 0.27 cm^{-1} (E_3 state), which are significantly higher than the coupling to the lowest energy exciton of LH-I. The couplings to state v_1 in (36) correspond to $\tau = 0.4(0.9)\text{ ps}$, which predicts transfer times that are more than an order of magnitude too short. One may conclude from this that, in fact, only the lowest energy exciton state of LH-I is involved in excitation transfer to the RC special pair. It is of interest to note that the coupling of the $E_{2,3}$ excitons of LH-I to the special pair states, in the absence

of the accessory BChls also leads to subpicosecond transfer times, but this coupling could play a role only if the respective exciton states are sufficiently populated. One needs to consider also the possibility that interruption of the LH-I ring, e.g., through Puf X, increases the oscillator strength of the lowest exciton state (see insert in Figure 7) such that excitation transfer $\text{LH-I} \rightarrow \text{RC}$ may occur on the 35 ps time scale without participation of the accessory BChls.

Intracomplex Transfer Revisited. We want to consider again the initial excitation transfer, namely, from the B800 BChls and from the 2A_g state of lycopene into the B850 band of LH-II.

The B800 band exhibits a dipolar coupling between nearest neighbors ($\text{Mg}-\text{Mg}$ distance 22 Å) of -44.2 cm^{-1} as predicted by (3), (5); the coupling to the nearest B850 cm^{-1} BChl ($\text{Mg}-\text{Mg}$ distance 19 Å) measures -67.6 cm^{-1} , i.e., is actually stronger than the intraband coupling. The excitation transfer $\text{B800} \rightarrow \text{B850}$ will reach higher energy exciton states, e.g., those with energy $E_{4,5} = 12\,251\text{ cm}^{-1}$ (816 nm) or $E_{6,7} = 12\,683\text{ cm}^{-1}$ (788 nm); the maximal coupling to those states, evaluated by means of (3), (5), for any individual B800 BChl is 43 and 31 cm^{-1} , respectively, which corresponds to exciton transfer times of 390 and 530 fs. These values are in qualitative agreement with the observed transfer time of 700 fs.^{38,40,41}

In case of the excitation transfer lycopene \rightarrow B850 through the 2A_g gateway state, coupling involves electron exchange and, accordingly, is local, i.e., involves only a single lycopene and a single BChl; each lycopene couples to B850 exciton states in an energy range of $13100\text{--}12500\text{ cm}^{-1}$ determined by the actual energy of the 2A_g state. In this range can be found the B850 exciton energies $E_{6,7}$, E_8 . The corresponding exciton states exhibit maximal coupling energies of $0.34x$, $0.24x$, where x is the unknown local electron exchange coupling between lycopene and BChl. For $x \approx 100\text{ cm}^{-1}$ an efficient excitation pathway with subpicosecond transfer times would be established.

5. Conclusion

We have presented above the combined structure of a photosynthetic reaction center with an integral light-harvesting system. The structure has been modeled according to the known structure of the basic components (RC and LH-II) as well as on the basis of a homologously modeled structure of LH-I with an ideal ring form. The detailed model provided an opportunity to apply the physics of exciton coupling and excitation transfer to describe the integral function of the PSU of purple bacteria and, thereby, to reveal the underlying mechanisms of this process. The description outlines a framework in which alternative PSU models, e.g., with different LH-I geometries, can be investigated.

The model structure exhibits a planar organization of the BChls involved in the intercomplex transfer: four central BChls of the RC are surrounded by a ring of 32 BChls, which itself is surrounded by multiple satellite rings containing 16 BChls each. We have demonstrated that the BChls, at least in the case of LH-II, are fixed in their orientation through ligation to histidines and through a network of hydrogen bonds. The latter network is indicative of the importance of a rigid orientation of the chromophores. In fact, the BChls assume an orientation that aligns the transition dipole moments of their Q_y states, the most relevant property for the light-harvesting function, in an optimal fashion, giving rise to strong exciton coupling in the light-harvesting complexes as well as sufficient coupling between complexes to achieve excitation transfer within a few picoseconds. The orientation seems to disfavor strongly out-of-plane components which would weaken in-plane coupling and give rise to radiative losses.

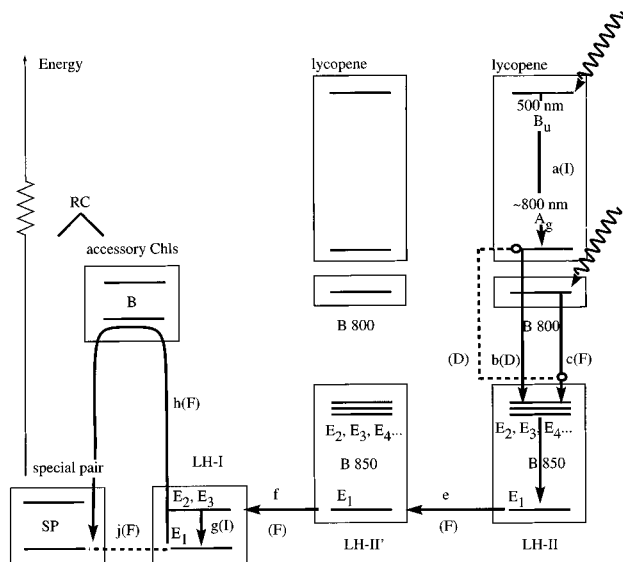


Figure 10. Scheme of the excitation transfer pathways of a 800 and a 500 nm photon in the bacterial PSU summarizing the effective Hamiltonian description in this study.

In addition to the mentioned coplanar BChl systems, there exist in the light-harvesting complexes further BChls and carotenoids that absorb light near 800 and 500 nm, respectively. We have traced how the light absorbed by these chromophores is funneled into the coplanar BChl system. Figure 10 depicts schematically the pathways along which the energy provided by 800 and 500 nm photons reaches eventually the RC. The 500 nm photon absorbed by lycopene populates fleetingly the second excited state, the B_u state. The chromophore relaxes to the lower lying A_g state within about 200 fs (step a) and has then an opportunity to couple to the coplanar (B850) BChl system through the Dexter mechanism (step b), the Förster mechanism being excluded due to the optically forbidden character of the A_g state.

The 16 B850 BChls in LH-II form a ring in which neighbors exhibit Mg–Mg distances of 8.9 and of 9.2 Å. The nature of the electronic excitation in such system has been intensely debated.⁶⁸ Instead of *ad hoc* assumptions we employed in our treatment an effective Hamiltonian chosen to match an extensive quantum chemical calculation.⁵⁶ The effective Hamiltonian, corresponding to a basis of single BChl excitations, exhibits interactions between neighboring BChls of 806 and 377 cm⁻¹, which implies a dimerized system with significant dimer–dimer interactions. In case of an ideal system without disorder, the resulting electronic excitations are delocalized and reflect the C_8 symmetry of the ring with the excitation at the lowest energy strictly forbidden and two degenerate excitations at the next higher energies, E_2 and E_3 , carrying all the oscillator strength.

Naturally, the question arises of to what extent inhomogeneous broadening affects the excitations of the ideal system. The answer is that a broadening as suggested by hole-burning experiments induces a small oscillator strength in the lowest excitation which should affect significantly the low-temperature behavior of the system, as reviewed in ref 68, but can be neglected for the purpose of describing the overall light-harvesting process.

The effective Hamiltonian description has also been applied to the B875 system of LH-I assuming an ideal ring geometry. The results show that the excitations of the LH-I system exhibit a behavior close to that of the LH-II system. The effective Hamiltonian has been extended also to incorporate essentially all BChls engaged in intercomplex excitation transfer. An appropriate choice of coupling elements permits one to include

also the RC BChls in an overall description. The Hamiltonian matrix elements reveal that the intercomplex transfer can be treated well in terms of perturbation theory, which provides then a straightforward route to determine the time scales of transfer into the B850 system of LH-II and of intercomplex excitation transfers LH-II → LH-II → LH-I → RC. The result yields then the following scenario for the entire transfer path of 500 and 800 nm photons discussed above.

The B800 system couples effectively into the higher ($E \geq E_{2,3}$) energy exciton states of the B850 system with transfer times of about 390–530 fs (step c). This transfer should be predominantly of the Förster type but might be enhanced through electron exchange involving the resonant $2A_g$ state of lycopene; the latter possibility requires further investigation.

The $2A_g$ state of lycopene provides the gateway for the 500 nm photons into the light-harvesting system. This state, like the B800 states, couples into the higher energy exciton states of the B850 ring of LH-II. In this case it has been demonstrated that coupling through short-range electron exchange to an individual B850 BChl can be effective, but a time scale has not been given due to uncertainties with the magnitude of local exchange coupling. To determine this coupling is a crucial goal. The relevance of this term is attested by the existence of light-harvesting proteins that involve a large number of carotenoids as antenna chromophores; a structure of one such protein, peridinin–chlorophyll–protein, has recently been solved⁶⁹ and exhibits close contacts between the carotenoids and BChls providing an opportunity for excitation transfer through electron exchange.

After transfer into the higher exciton states of the B850 system of LH-II, thermal relaxation leads to the predominant population of the lowest energy (E_1) exciton. The degree of occupancy depends sensitively on the exact gap $E_2 - E_1$, which seems to be widened through higher energy excitations not included in the effective Hamiltonian treatment. The calculations in ref 56 predict a 90% occupancy of the E_1 state. Low-temperature spectroscopy, as reviewed in ref 68, and hole-burning spectroscopy as in ref 61 might shed further light on the $E_2 - E_1$ gap. In the following we will assume, as a working hypothesis, that the thermalized exciton bands are found solely in the lowest energy state. Occupancy of higher exciton states would increase the coupling strength for the passage of excitations to the RC; such states may, however, fluoresce light and, thereby, decrease the efficiency of light harvesting, but this would only occur if the excitation transfer steps are too slow. In fact, the main reason why one wishes to invoke a chief role of the E_1 level is the striking C_8 symmetry of LH-II: asking to what degree this symmetry could assume functional importance leads one naturally to note the vanishing or very small oscillator strength of the E_1 exciton that is tied to a symmetry center.

One may consider the lowest exciton state, due to its weak oscillator strength, as an ineffective carrier of exciton transfer. However, we have shown above that the state exhibits strong couplings for the LH-II → LH-II → LH-I → RC transition, i.e., for the steps e, f, and h in Figure 10. The overall oscillator strength is not material since the couplings break the symmetry of the exciton systems such that even the optically forbidden E_1 level exhibits sufficient coupling. In the case of the LH-II → LH-II transfer the E_1 levels define both the initial and the final states. In the case of the LH-II → LH-I transfer, the transfer reaches the $E_{2,3}$ levels. In the case of the LH-I → RC transfer the initial state lies at 11 335 cm⁻¹, which lies about 225 cm⁻¹ below the 865 nm absorption maximum of the lowest (allowed) exciton state of the RC BChls. This gap might be

bridged through vibronic coupling, widening the spectrum of the RC, or a lower lying special pair charge transfer state might be the actual recipient state. In this case our description for the LH-I \rightarrow RC transfer needs to be modified to include the respective state in an effective Hamiltonian.

A startling suggestion resulting from our calculations has been a key role of the accessory BChls as mediators of the LH-I \rightarrow RC transfer. The accessory BChls have attracted much attention as possible mediators of the primary electron transfer in the RC. A recent discussion of this role is found in ref 70. The focus on the role of the RC to initiate electron transfer might have diverted attention from its other function, to collect excitation energy from the surrounding light-harvesting system, for which task the accessory BChls seem to be naturally attuned. We have stated explicitly above the Hamiltonian which couples the lowest energy (E_1) LH-I exciton to the RC BChls. The elements of this Hamiltonian and the number (five) of excitations employed should be subject of further improvements, and the suggested role of the accessory BChls should be scrutinized. We have stated above that the E_2 and E_3 exciton levels of LH-I exhibit a stronger coupling to the RC BChls than the E_1 level such that thermal activation may be an alternative route or actually the main route of LH-I \rightarrow RC excitation transfer.

The integral structure of the PSU and the corresponding effective Hamiltonian description explain a remarkable number of features of the light-harvesting process in purple bacteria. It should be stated that the Hamiltonian employed had no adjustable parameters; it is derived entirely from the quantum chemical calculation in ref 56 as well as from the geometry of the aggregate of RC, LH-I, and LH-II. In this regard the explanations regarding transfer times and mechanism derive from first principles. Nevertheless, the model of the PSU and the effective Hamiltonian treatment leave many question unanswered; in fact, new questions are raised.

One of the new questions that calls for an answer concerns the way by which the light-harvesting complexes aggregate in the photosynthetic membrane and how the size of the rings is determined. A related question is how the light-harvesting complexes are actually arranged in the membrane, i.e., if the crystal structures and the structures seen by electron microscopy are realized *in situ* under conditions of dim and intense light. A question touched on by our study regards the existence of a symmetry center for LH-II and LH-I. Such symmetry centers have been observed for all light-harvesting complexes.^{21,22,26,27,69} This might be neither an accident nor a matter of evolutionary strategy, e.g., gene duplication, but rather may have a mechanistic basis.

The effective Hamiltonian description suggested here should be extended to include double excitations in order to allow the description of pump-dump experiments.⁷¹ The physics of intracomplex processes needs to be better understood: What is the magnitude of the coupling between the $2A_g$ lycopene state and BChls? What is the effect of off-diagonal disorder, i.e., disorder produced by the thermal fluctuation of BChl position and orientation through the dipolar couplings (eq 3)? The availability of a structural model will impel many further studies of light harvesting; we have provided the necessary geometrical details and couplings to pave the way for further investigations by others.

An open question remains, i.e., what causes the spectral red shift of BChls in the pigment-protein complexes. Absorption spectra of BChl-a peaks at 772 nm in organic solvent.⁶⁰ As has been observed, the peak positions red shift to various extents in LH-II, LH-I, and the RC, which is vital to the formation of excitation transfer cascade in the bacterial PSU. Our calcula-

tions suggest that excitonic interactions are responsible for a major part of the spectral red shift, but that BChl-protein interactions shifting the site energies of individual BChls must contribute significantly, too.

Acknowledgment. The authors express their gratitude to Mike Zerner for providing information on the exciton states in an aggregate of chlorophylls modeling the B850 system of LH-II. The authors thank Andrew Dalke for help in rendering images of bacteriochlorophylls with VMD and acknowledge the Carver Charitable Trust, the National Institutes of Health (P41RR05969), and the National Science Foundation (NSF BIR 9318159 and NSF BIR-94-23827(EQ)) for financial support. We are grateful for a MetaCenter Allocation for computational resources at the San Diego Supercomputer Center (MCA93S028P).

References and Notes

- (1) van Grondelle, R.; Dekker, J.; Gillbro, T.; Sundstrom, V. *Biochim. Biophys. Acta* **1994**, *1187*, 1.
- (2) Fleming, G. R.; van Grondelle, R. *Phys. Today* **1994**, *47*, 48.
- (3) Knox, R. S. In *Primary Processes of Photosynthesis*; Barber, J., Ed.; Elsevier: Amsterdam, 1977; p 55.
- (4) Sauer, K. *Bioenergetics of Photosynthesis*; Govindjee, Ed.; Academic Press: New York, 1975; p 115.
- (5) Emerson, R.; Arnold, W. J. *Gen. Physiol.* **1932**, *16*, 191.
- (6) Duysens, L. N. M. Transfer of Excitation Energy in Photosynthesis. Ph.D. Thesis, Utrecht, 1952.
- (7) Duysens, L. N. M. *Prog. Biophys. Mol. Biol.* **1964**, *14*, 1.
- (8) Parson, W. W. In *The Photosynthetic Bacteria*; Clayton, R. K., Sistrom, W. R., Eds.; Plenum: New York, 1978; p 317.
- (9) Borisov, A. Y.; Godik, V. I. *Biochim. Biophys. Acta* **1973**, *301*, 227.
- (10) Mauzerall, D.; Greenbaum, N. L. *Biochim. Biophys. Acta* **1989**, *974*, 119.
- (11) Freiberg, A. In *Anoxygenic Photosynthetic Bacteria*; Blankenship, R. E., Madigan, M. T., Bauer, C. E., Eds.; Kluwer Academic Publishers: Dordrecht, 1995; p 385.
- (12) Papiz, M. Z.; Prince, S. M.; Hawthornthwaite-Lawless, A. M.; McDermott, G.; Freer, A. A.; Isaacs, N. W.; Cogdell, R. J. *Trends Plant Sci.* **1996**, *1*, 198.
- (13) van Grondelle, R.; Sundstrom, V. In *Photosynthetic Light-Harvesting Systems*; Scheer, H., Ed.; Walter de Gruyter & Co.: Berlin, New York, 1988; p 403.
- (14) Zuber, H.; Brunisholz, R. A. In *Chlorophylls*; Scheer, H., Ed.; CRC Press: Boca Raton, FL, 1991; p 627.
- (15) Williams, W. P. In *Primary Processes of Photosynthesis*; Barber, J., Ed.; Elsevier: Amsterdam, 1977; p 100.
- (16) Krauss, N.; Schubert, W.-D.; Klukas, O.; Fromme, P.; Witt, H. T.; Saenger, W. *Nat. Struct. Biol.* **1996**, *3*, 965.
- (17) Borisov, A. Y. In *The Photosynthetic Bacteria*; Clayton, R. K., Sistrom, W. R., Eds.; Plenum: New York, 1978; p 323.
- (18) Drews, G.; Golecki, J. R. In *Anoxygenic Photosynthetic Bacteria*; Blankenship, R. E., Madigan, M. T., and Bauer, C. E., Eds.; Kluwer Academic Publishers: Dordrecht, 1995; p 231.
- (19) Deisenhofer, J.; Epp, O.; Miki, K.; Huber, R.; Michel, H. *Nature* **1985**, *318*, 618.
- (20) Allen, J. P.; Yeates, T. O.; Komiya, H.; Rees, D. C. *Proc. Natl. Acad. Sci. U.S.A.* **1987**, *84*, 6162.
- (21) McDermott, G.; Prince, S. M.; Freer, A. A.; Hawthornthwaite-Lawless, A. M.; Papiz, M. Z.; Cogdell, R. J.; Isaacs, N. W. *Nature* **1995**, *374*, 517.
- (22) Koepke, J.; Hu, X.; Muenke, C.; Schulten, K.; Michel, H. *Structure* **1996**, *4*, 581.
- (23) Hawthornthwaite, A. M.; Cogdell, R. J. In *Chlorophylls*; Scheer, H., Ed.; CRC Press: Boca Raton, FL, 1991; p 493.
- (24) Germeroth, L.; Lottspeich, F.; Robert, B.; Michel, H. *Biochemistry* **1993**, *32*, 5615.
- (25) Zuber, H. *Photochem. Photobiol.* **1985**, *42*, 821.
- (26) Savage, H.; Cyrklafl, M.; Montoya, G.; Kuhlbrandt, W.; Sinning, I. *Structure* **1996**, *4*, 243.
- (27) Karrasch, S.; Bullough, P. A.; Ghosh, R. *EMBO J.* **1995**, *14*, 631.
- (28) Cogdell, R. J.; Frank, H. A. *Biochim. Biophys. Acta* **1987**, *895*, 63.
- (29) Schulten, K.; Ohmine, I.; Karplus, M. *J. Chem. Phys.* **1976**, *64*, 4422.
- (30) Tavan, P.; Schulten, K. *Phys. Rev. B* **1987**, *36*, 4337.
- (31) Zuber, H. *Trends Biochem. Sci.* **1986**, *11*, 414.

(32) Boonstra, A. F.; Germeroth, L.; Boekema, E. J. *Biochim. Biophys. Acta* **1994**, *1184*, 227.

(33) Ermler, U.; Fritzsch, G.; Buchanan, S. K.; Michel, H. *Structure* **1994**, *2*, 925.

(34) Hu, X.; Xu, D.; Hamer, K.; Schulten, K.; Koepke, J.; Michel, H. *Protein Sci.* **1995**, *4*, 1670.

(35) Hu, X.; Schulten, K. In preparation.

(36) Olsen, J.; Sturgis, J. N.; Hunter, C. N.; Robert, B. *Biochemistry*, in preparation.

(37) Robert, B. and Lutz, M. *Biochim. Biophys. Acta* **1985**, *807*, 10.

(38) Joo, T.; Jia, Y.; Yu, J.-Y.; Jonas, D., and Fleming, G. *J. Phys. Chem.* **1996**, *100*, 2399.

(39) Shreve, A. P.; Trautman, J. K.; Frank, H. A.; Owens, T. G.; Albrecht, A. C. *Biochim. Biophys. Acta* **1991**, *1058*, 280.

(40) Hess, S.; Chachisvilis, M.; Timpmann, K.; Jones, M. R.; Fowler, G. J. S.; Hunter, C. N.; Sundstrom, V. *Proc. Natl. Acad. Sci. U.S.A.* **1995**, *92*, 12333.

(41) Kennis, J. T. M.; Streltsov, A. M.; Aartsma, T. J.; Nozawa, T.; Amesz, J. *J. Phys. Chem.* **1996**, *100*, 2438.

(42) Monshouwer, R.; Zarate, I. O. d.; van Mourik, F.; van Grondelle, R. *Chem. Phys. Lett.* **1995**, *246*, 341.

(43) Förster, T. *Ann. Phys. (Leipzig)* **1948**, *2*, 55.

(44) Dexter, D. L. *J. Chem. Phys.* **1953**, *21*, 836.

(45) Gouterman, M. *J. Mol. Spectrosc.* **1961**, *6*, 138.

(46) Weiss, C. *J. Mol. Spectrosc.* **1972**, *44*, 37.

(47) Fowler, G. J.; Visschers, R. W.; Grief, G. G.; van Grondelle, R.; Hunter, C. N. *Nature* **1992**, *355*, 848.

(48) Hess, S.; Visscher, K. J.; Pullerits, T.; Sundstrom, V.; Fowler, G. J. S.; Hunter, C. N. *Biochemistry* **1994**, *33*, 8300.

(49) Koyama, Y.; Kuki, M.; Andersson, P. O., and Gillbro, T. *Photochem. Photobiol.* **1996**, *63*, 243.

(50) Frank, H. A.; Cogdell, R. J. *Photochem. Photobiol.* **1996**, *63*, 257.

(51) Hudson, B. S.; Kohler, B. E.; Schulten, K. In *Excited States*; Lim, E. C., Ed.; Academic Press: New York, 1982; Vol. 6, p 1.

(52) Kandori, H.; Sasabe, H.; Mimuro, M. *J. Am. Chem. Soc.* **1994**, *116*.

(53) Bondarev, S. L.; Tikhomirov, S. A.; Bachilo, S. M. *SPIE* **1990**, *1403*, 497.

(54) Damjanovic, A.; et al. To be submitted.

(55) Ricci, M.; Bradforth, S. E.; Jimenez, R.; Fleming, G. R. *Chem. Phys. Lett.* **1996**, *259*, 381.

(56) Zerner, M. C.; Cory, M. G.; Hu, X.; Schulten, K. To be published.

(57) Sauer, K.; Smith, J. R. L.; Schultz, A. J. *J. Am. Chem. Soc.* **1966**, *88*, 2681.

(58) Pearlstein, R. M. *Photosynth. Res.* **1992**, *31*, 213.

(59) Zerner, M. C. *ZINDO, A General Semi-Empirical Program Package*, Department of Biochemistry, University of Florida.

(60) Oelze, J. *Methods Microbiol.* **1985**, *18*, 257.

(61) Wu, H.-M.; Reddy, N. R. S.; Small, G. *J. Phys. Chem. B* **1997**, *101*, 651.

(62) Dracheva, T. V.; Novoderezhkin, V. I.; Razjivin, A. *FEBS Lett.* **1996**, *387*, 81.

(63) Leupold, D.; Stiel, H.; Teuchner, K.; Nowak, F.; Sandner, W.; Ucker, B.; Scheer, H. *Phys. Rev. Lett.* **1996**, *77*, 4675.

(64) Somsen, O. J. G.; van Grondelle, R.; van Amerongen, H. *Biophys. J.* **1996**, *71*, 1934.

(65) Reddy, N. R. S.; Picorel, R.; Small, G. *J. Phys. Chem.* **1992**, *96*, 6458.

(66) Eccles, J.; Honig, B.; Schulten, K. *Biophys. J.* **1988**, *53*, 137.

(67) Visscher, K. J.; Bergstrom, H.; Sundstrom, V.; Hunter, C. N., van Grondelle, R. *Photosynth. Res.* **1989**, *22*, 211.

(68) Monshouwer, R.; van Grondelle, R. *Biochim. Biophys. Acta* **1996**, *1275*, 70.

(69) Hofmann, E.; Wrench, P.; Sharples, F.; Hiller, R.; Welte, W.; Diederichs, K. *Science* **1996**, *272*, 1788.

(70) Makri, N.; Sim, E.; Makarov, D. E.; Topaler, M. *Proc. Natl. Acad. Sci. U.S.A.* **1996**, *93*, 3926.

(71) Pullerits, T.; Chachisvilis, M.; Sundstrom, V. *J. Phys. Chem.* **1996**, *100*, 10787.

(72) Humphrey, W. F.; Dalke, A.; Schulten, K. *J. Mol. Graphics* **1996**, *14*, 33.